Acta Neuropathologica Communications

RESEARCH

Open Access

Chaperone mediated autophagy is deficient in spinal motoneurons of ALS patients with TDP-43 proteinopathy

Daniel Garrigos[1], Marta Martinez-Morga[1], Ana Pombero[1], Raquel García-Lopez[1], Diego Pastor[2], Dolores Riquelme[3], Miguel Blanquer[3], Francisca Iniesta[4], Rut Valdor[3], Emilio Geijo-Barrientos[1], Gunnar Hargus[5], José María Moraleda[3] and Salvador Martínez[1,6*]

Abstract

Amyotrophic Lateral Sclerosis (ALS) is a progressive neurodegenerative disease characterized by the selective loss of motor neurons (MNs), ultimately resulting in paralysis and respiratory failure within 3 to 5 years of onset. Fewer than 10% of ALS cases are familial (fALS), while the vast majority are sporadic (sALS) with an unknown etiology. A pathological hallmark of ALS is the accumulation of misfolded TDP-43 protein aggregates within MNs. Although TDP-43 is known to be degraded via chaperone-mediated autophagy (CMA), the status of CMA activity in sALS has not been previously explored. To investigate this, we analyzed CMA in human spinal cord tissue by assessing the expression of LAMP2A, a key lysosomal receptor and marker of CMA activity. In control samples, spinal cord MNs exhibited robust LAMP2A expression. In contrast, MNs from sALS patients showed a marked reduction in LAMP2A levels, coinciding with the presence of TDP-43 pathology. Notably, analysis of LC3, a marker of macroautophagy, revealed no significant differences in expression between control and sALS MNs. Interestingly, MNs within the Onuf's nucleus, a population known to be resistant to degeneration in ALS, retained normal LAMP2A expression and did not exhibit TDP-43 aggregation in sALS cases. These findings demonstrated that CMA is essential for the clearance of TDP-43 in spinal cord MNs and that its dysfunction may contribute to the pathogenesis of sALS. Furthermore, the high dependence of spinal cord MNs on CMA activity may underlie their selective vulnerability to degeneration when CMA is impaired, and highlight CMA enhancement as a promising therapeutic strategy to restore proteostasis and prevent MN degeneration in ALS.

Keywords Motor neurodegeneration, sALS, Differential vulnerability to neurodegeneration, Chaperone mediated autophagy, Human motoneurons

*Correspondence:
Salvador Martínez
smartinez@umh.es
[1]Instituto de Neurociencias (UMH-CSIC), San Juan de Alicante, Alicante, Spain
[2]Sports Research Centre, Department of Sport Sciences, Miguel Hernández University, Elche, Spain
[3]Instituto Murciano de Investigación Biosanitaria Pascual Parrilla (IMIB), Murcia University, Murcia, Spain
[4]Universidad Católica de Murcia (UCAM), Murcia, Spain
[5]Institut für Neuropathologia. Universitätsklinikum Münster, München, Germany
[6]Instituto de Investigación Sanitaria y Biomédica de Alicante (ISABIAL) and CIBER de Salud Mental ISCIII (CIBERSAM), Alicante, Spain

Introduction

Amyotrophic lateral sclerosis (ALS) is a fatal neurodegenerative disease characterized by the progressive loss of motor neurons (MNs) in the primary motor cortex and spinal cord (SC) [15, 75]. Most patients succumb within 3–5 years due to progressive palsy and respiratory failure [64]. The global prevalence and incidence are estimated at 4.1–8.4 per 100,000 individuals and 0.6–3.8 per 100,000 person-years, respectively [54], with approximately 30,000 deaths reported annually [72]. ALS arises from a complex interplay of genetic and environmental factors [60], and manifests in familial (fALS) and sporadic (sALS) forms [91]. More than 20 genetic mutations have been implicated, with *C9ORF72*, *FUS*, *TARDBP*, and *SOD1* being the most frequently involved [75].

Regardless of etiology or site of onset, ALS is a predominantly MN-selective neurodegenerative disorder for reasons that remain unclear. This selectivity has been attributed to several intrinsic features of MNs, including their large size, high metabolic demands, dependence on mitochondrial integrity, vulnerability to excitotoxicity, disrupted intracellular calcium homeostasis, and impaired ubiquitin–proteasome system function [14, 67, 75]. A bottom-up pathogenic model, retrograde neuropathy originating at neuromuscular terminals, may account for the preferential degeneration of spinal MNs and the potential for trans-synaptic involvement of the primary motor cortex [65, 67]. Moreover, differences in neuromuscular junction architecture may underlie the relative resistance of certain MN subpopulations, such as oculomotor and Onuf's nuclei, although this remains experimentally unverified [14].

Current therapeutic options for ALS remain limited. Riluzole, the first approved drug, extends survival by only 6–19 months [2]. Edaravone received FDA approval in 2017 [90], but failed to show efficacy in an independent clinical trial in Italy [56]. More recently, antisense oligonucleotide therapies have been developed for fALS with SOD1 mutations [80]. Tofersen, approved in SOD1 fALS following a phase III trial, did not yield significant clinical improvement but showed encouraging biomarker responses, including reductions in cerebrospinal fluid SOD1 protein and plasma neurofilament light chain (NfL) levels [61]. Similarly, Relyvrio, initially approved for slowing ALS progression, was later withdrawn after a failed phase III trial [4, 68]. Given the absence of effective treatments for ALS, there is an urgent need for further preclinical research and improved drug-target identification.

Among the cellular pathways increasingly implicated in ALS pathogenesis, autophagy plays a central role in maintaining protein homeostasis and cellular integrity [49, 82, 87]. This multi-step process involves the lysosomal degradation and recycling of intracellular components, including aberrant proteins and damaged organelles [82]. Three types of autophagy are described in mammals: macroautophagy (MA), microautophagy, and chaperone-mediated autophagy (CMA). While MA and microautophagy involve bulk degradation and direct lysosomal delivery of cargo, respectively [1], CMA selectively targets proteins bearing a KFERQ-like motif. These are recognized by the HSC70 chaperone and delivered to the lysosomal receptor LAMP2A, the key limiting factor for CMA in the neurons [13, 42, 73, 77].

Notably, TDP-43, a nuclear RNA-binding protein involved in RNA processing, genome integrity, and mRNA metabolism [5, 31, 66], contains the KFERQ-like motif [48]. In approximately 95% of ALS cases, TDP-43 is mislocalized, forming phosphorylated and ubiquitinated cytoplasmic aggregates that are hallmark features of spinal MN pathology [18, 22, 23, 66]. Although these aggregates are prominent in sALS, mutations in TARDBP and C9orf72 can also lead to TDP-43 proteinopathy [76]. Clearance of TDP-43 aggregates is critical to mitigate their cytotoxicity and has been linked to both the ubiquitin–proteasome system and MA [24, 66, 86]. Moreover, reducing TDP-43 levels in ALS mouse models improves motor deficits, suggesting that motoneuronal dysfunction may be at least partially reversible [43]. It has been proved in experimental models that MA activation, for instance through mTOR inhibition, enhances TDP-43 turnover and cell viability [32, 33].

Given the role of TDP-43 in ALS and its potential recognition by CMA, we investigated LAMP2A expression, a key marker of CMA in human SCs [48]. We analyzed SC tissue from six control subjects (n = 6; 3 females, 3 males) and ten sALS patients (n = 10; 6 females, 4 males), which exhibited varying degrees of TDP-43 proteinopathy. In control SCs, we observed intense LAMP2A expression in MNs across all regional levels. In contrast, sALS SC samples showed a marked reduction in LAMP2A expression in MNs, both in early pathological stages, characterized by nuclear TDP-43 clearance and granular cytoplasmic aggregates, and in advanced stages with dense cytoplasmic TDP-43 inclusions. Interestingly, Onuf's nucleus MNs, which are relatively spared in ALS [14, 58], displayed strong LAMP2A expression and lacked TDP-43 pathology. Recent studies in animal models have identified CMA as a key regulator of excitability in neurons, highlighting its potential relevance to MNs vulnerability in sALS [46]. These findings suggest that CMA dysfunction may contribute to the selective vulnerability of MNs in ALS and underscore a potential protective role of preserved CMA activity in resistant MN populations.

M&M

Human tissue processing

Human control samples without neurological disorder ($n = 6$ SC) were obtained from anonymous donations through the Anatomy Innovation Service of Miguel Hernandez University Medical School, which provides administrative and ethical support, with the approval of the Institutional Review Board. Samples and data from patients included in this study ($n = 10$ SC) were provided by the Biobank IMIB (National Registry of Biobanks B. 0000859) (PT20/00109), integrated in the Platform ISCIII Biobanks and Biomodels and they were processed following standard operating procedures with the appropriate approval of the Ethics and Scientific Committees. Voluntary donations were obtained from patients included in the Phase I and II of clinical trial nº EudraCT:2006-00309612, NCT00855400 and EC 07/90,762, NCT01254539 (Supplementary Table 1).

Tissue Preparation and immunohistochemical staining

Spinal cords were fixed in 10% formalin (Sigma-Aldrich, Germany) for 5 days at room temperature. Following fixation, the SC was transversely trimmed into tissue slides (TS) 5–7 mm thick and labelled in a rostro-caudal order into progressive cervical, thoracic, lumbar, or sacral regions (Supplementary Fig. 1). TS underwent a progressive dehydration process in ethanol, followed by butanol and were subsequently embedded in paraffin. Transversal sections, 7–10 µm thick, were then obtained from four selected TS at each SC region, covering the entire region, and mounted on microscopy slides (MS) in 20 parallel series (Supplementary Fig. 1).

Spinal cords were processed to paraffin embedding and sectioning sections following the protocol described in Supplementary Fig. 1. MS were processed by Hematoxylin-Eosin (H&E, serie 1), Cresyl violet (CV, serie 2), and immunohistochemistry (series 3–11). We conducted immunohistochemical analysis on subsequent parallel series of MS from cervical segments C3-6 (n = 20), thoracic segments T8-11 (n = 20), lumbar segments L2-5 (n = 20), and sacral segments S1-4 (n = 20) of control and sALS SCs. To minimize experimental bias in the data of ALS patients, T2–T6 segments were excluded because 7 patients had received intraspinal autologous graft of mononuclear bone marrow cells (MNBMc) in the T3–T5 [10], intrathecal MNBMc graft, or intrathecal administration of saline solution, as placebo group (clinical trials (CT) NCT00855400 and NCT04849065, Phase I and II; Supplementary Table 1). Finally, one patient was not included in Phase II CT and was classified as a not treated ALS patient (Supplementary Table 1). Our previous pathological data from the Phase I CT showed no significant modifications in non-experimental segments [11], therefore, the rostral and caudal segments relative to T2–T7 were considered affected in accordance with the natural progression of the disease in each patient.

Immunohistochemistry procedures were described in Blanquer et al., [11]. Briefly, sections were treated with primary antibodies, diluted in EnVision FLEX Antibody Diluent (DAKO, Denmark), 24 h at 4 °C (Supplementary Table 2). Following primary antibody incubation, sections were incubated 2 h with the appropriate biotinylated secondary antibody (Supplementary Table 2). Then, sections were incubated with Avidin–Biotin Complex for 1 h (ABC kit, Vector Laboratories CA-94010). For colorimetric detection (brown), the tissue was incubated with 1% 3,3'-Diaminobenzidine (DAB; Vector Laboratories SK-4100) and 0.0018% H2O2 in PBS. For double immunohistochemistry with anti-TDP 43/anti-ChAT and anti-TDP-43/anti-LAMP2A, anti-TDP-43 was incubated with 1% 3,3'-Diaminobenzidine (DAB; Vector Laboratories SK-4100), 0.025% ammonium nickel sulfate hexahydrate, and 0.0018% H2O2 in PBS for colorimetric detection (black). For double immunochemistry with anti-GFAP/anti-IBA1, anti-IBA1 was processed to obtain a black color. For immunofluorescence experiments, after primary antibody incubation, sections were washed in PBST and incubated for 2 hours at room temperature with an Alexa Fluor 488-conjugated goat anti-rabbit secondary antibody (1:500; Invitrogen, USA). Sections series processed in parallel without primary or secondary antibodies did not show any specific or non-specific labeling (Supplementary Fig. 2). Finally, the sections were dehydrated and mounted in Eukitt (O.Kindler GmbH and CO, Freiburg), whereas immunofluorescence sections were mounted using Mowiol mounting medium (Sigma-Aldrich).

Microscopy and statistical analysis

Images were captured using an optical microscope (Leica CTR6000) and were utilized to assess the percentage of cellular area expressing various markers, including LAMP2A, LC3, and GBA (see below). After identifying MNs in ventro-medial and ventro-lateral columns (where more MNs were identified in ALS patients), the ImageJ program was employed to quantify the percentage of area expressing LAMP2A, LC3, and GBA relative to the total cell area ($n = 20$ MNs/marker in each group). Statistical analysis comparing sALS and control samples was performed using Sigmaplot v11.0 software. The data were presented as mean values ± standard error (SE), and pairwise comparisons between sALS and control samples (attending: gender, segmental level and MNs column) were conducted using the Student's t-test. Graphs and statistical visualizations were generated using GraphPad Prism version 10 (GraphPad Software, San Diego, CA). A significance level of $p < 0.05$ was considered statistically

Figure 1

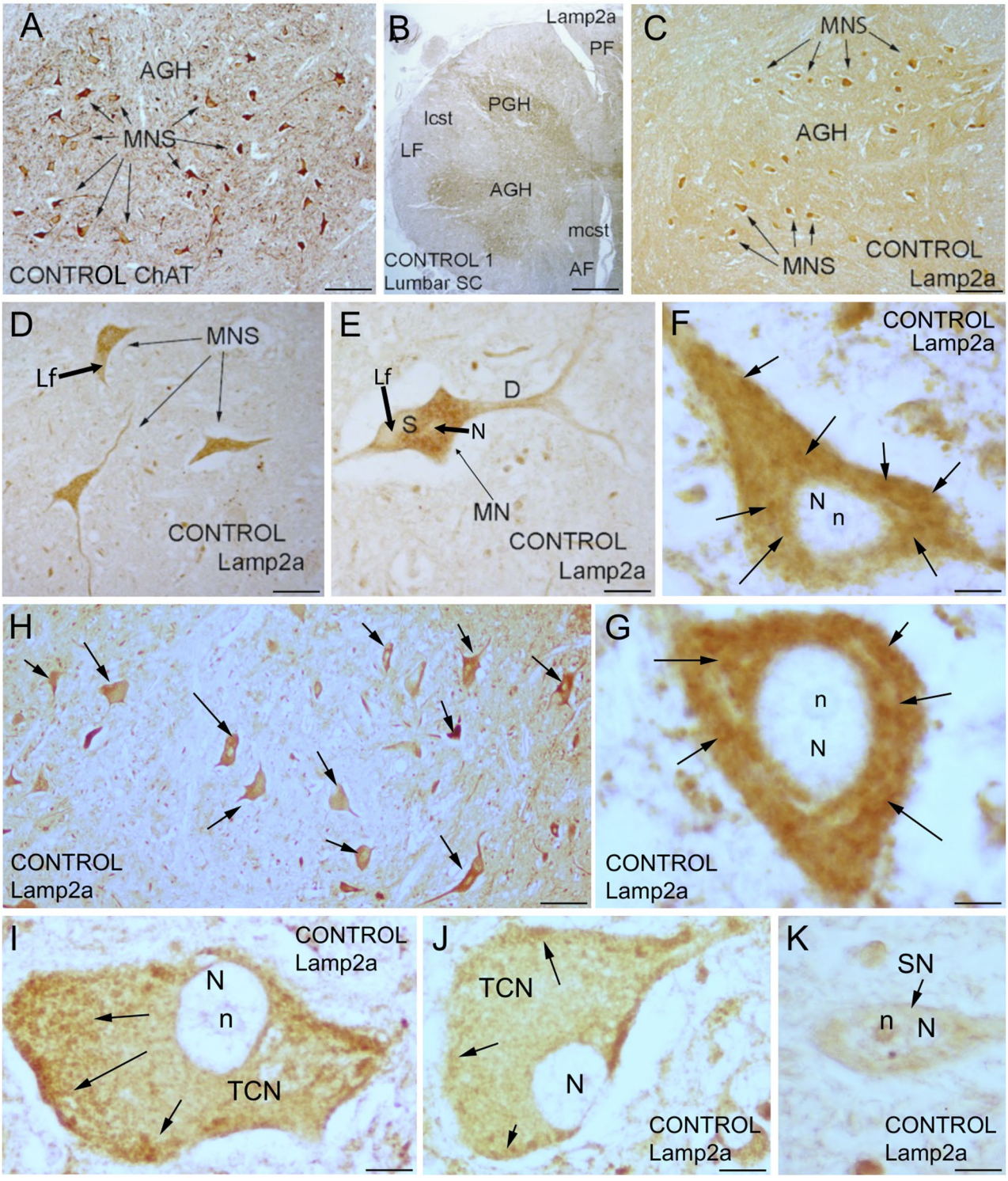

Fig. 1 (See legend on next page.)

significant, with $^{*}p < 0.05$, $^{**}p < 0.01$, and $^{***}p < 0.001$ denoting different levels of significance. Additionally, to validate these findings with higher sensitivity, quantitative immunofluorescence was performed for LAMP2A expression. For this purpose, 16-bit fluorescence images were acquired to ensure a high dynamic range and prevent signal saturation. A total of 10 MNs per subject were analyzed in a cohort of 4 control subjects ($n = 40$ total

(See figure on previous page.)

Fig. 1 ChAT-positive cells and LAMP2A expression in control motor neurons (MNs). **a** Distribution of ChAT-positive MNs in the lumbar spinal cord. **b**–**k** LAMP2A immunoreactivity in neurons of the control lumbar spinal cord. **b** Low-magnification image showing the localization of gray and white matter regions in spinal cord sections. **c** High LAMP2A expression was selectively observed in MNs of the anterior gray horn (AGH) (arrows). **d**–**h** MNs in the anterior gray horn exhibited a distinct, highly LAMP2A-immunopositive puncta pattern in the perinuclear cytoplasm (arrows in f and g). **i**–**j** Neurons of Clarke's thoracic column showed no LAMP2A immunostaining, or only scattered puncta expression localized to the cell body periphery (arrows). **k** Sensory neurons in the dorsal horn did not show LAMP2A immunoreactivity (arrow). Abbreviations: AF = Anterior funiculus, AGH = Anterior gray horn, lcst = Lateral corticospinal tract, Lf = Lipofuscin, MNs = Motoneurons, PF = Posterior funiculus, PGH = Posterior gray horn, S = Neuronal soma, N = Neuronal nucleus, n = Neuronal nucleolus, SN = Sensory neuron, TCN = Clarke's thoracic column neurons. Scale bar: A: 300 µm; B: 3 mm; C: 300 µm; D: 120 µm; E: 60 µm; F, G: 20 µm; H: 160 µm; I, J, K: 20 µm

MNs) and 5 ALS patients ($n = 50$ total MNs). Fluorescence intensity was quantified using the Corrected Total Cell Fluorescence (CTCF) method, calculated as follows: (IntDen - (Area * Mean Background)). The background value was determined by the mean fluorescence of three representative regions adjacent to each MN. Statistical analysis comparing sALS and control samples was performed using Sigmaplot v11.0 software for DAB samples and GraphPad Prism version 10 for immunofluorescence data. The data were presented as mean values ± standard error (SE), and pairwise comparisons between sALS and control samples (attending: gender, segmental level and MNs column) were conducted using the unpaired, two-tailed Student's t-test. Graphs and statistical visualizations were generated using GraphPad Prism version 10 (GraphPad Software, San Diego, CA). A significance level of $p < 0.05$ was considered statistically significant, with $^{*}p < 0.05$, $^{**}p < 0.01$, and $^{***}p < 0.001$ denoting different levels of significance.

Results

Spinal motoneurons exhibit elevated expression levels of LAMP2A.

Given that TDP-43 is a potential substrate for CMA [37, 66], we investigated LAMP2A expression, the rate-limiting component of CMA [73], in spinal MNs.

To investigate LAMP2A expression in the human SC, we conducted immunohistochemical analyses on sections from C3–C4, T8–T9, L3–L4, and S2–S3 segments (n = 10 slides per segment) obtained from control SC (n = 6; Supplementary Table 1). MNs were identified based on their distinct morphological features observed with H&E and CV staining, as well as their immunoreactivity for choline acetyltransferase (ChAT) (Fig. 1a). In parallel slides we observed robust and specific LAMP2A expression in MNs across all SC segments (Fig. 1b–g). The immunoreactivity exhibited a puncta perinuclear pattern within the MN cytoplasm, consistent with lysosomal membrane localization of LAMP2A [77] (Fig. 1e-h). Additionally, most MNs also contained lipofuscin granules that were immunonegative for both ChAT and LAMP2A (Fig. 1d, e; Supplementary Fig. 3a–d).

In contrast, LAMP2A immunoreactivity was markedly lower in other neuronal populations, including Clarke's column neurons (TCNs; Fig. 1i, j; Supplementary Fig. 3e) and dorsal horn sensory neurons (SNs; Fig. 1k); Supplementary Fig. 3f). In TCNs, LAMP2A-positive puncta were distributed throughout the cytoplasm rather than showing a perinuclear concentration as seen in MNs (Fig. 1i, j). Additionally, glial cells (GCs) exhibited minimal LAMP2A immunoreactivity (Supplementary Fig. 3d, f–h).

Then, we explored potential age- and sex-related differences in CMA by comparing SC samples from Control 1 and 6, derived from 64- and 62-year-old females, respectively, with Control 3 and 5, obtained from 53-year-old males (Fig. 2a). Our analysis did not reveal significant differences in LAMP2A expression among these SC samples. Notably, despite the male samples being approximately 10 years younger than the female samples, LAMP2A expression levels were comparable. Furthermore, comparison of SC samples from Control 1 and 6 with Control 4 (a 70-year-old female, almost 10 years older) also showed no substantial differences in LAMP2A expression (data not shown). Therefore, do not reveal age-related or sex-specific differences in LAMP2A expression in MNs.

These findings indicate that spinal MNs selectively express high levels of LAMP2A, suggesting heightened CMA activity.

Spinal motoneurons of sALS patients exhibit low expression levels of LAMP2A.

To analyze CMA activity in spinal MNs of sALS patients, we performed LAMP2A immunohistochemistry on sections from C3-C4, T8-T9, L3-L4, and S2-S3 segments of sALS patient's SC ($n = 10$; Supplementary Table 1. In sALS SCs, cervical, lumbar, and sacral segments exhibited a greater number of detectable MNs based on morphological and immunohistochemical criteria (a mean of 9–12 MNs/section, 12–17 MN/section, and 5–10 MN/section, respectively) compared to thoracic segments (0–3 MN/section). Consequently, we increased in our study the number of thoracic slides ($n = 20$) to ensure at least 20 thoracic MNs were analyzed in each patient, along with 20 MNs from other SC regions ($n = 10$ from each segment), which were then compared with the same number of control MNs. In all cases of sALS SC, LAMP2A immunopositivity was notably weak in most of the MNs (Figs. 2 and 3). While the majority of MNs from sALS patients showed a significantly

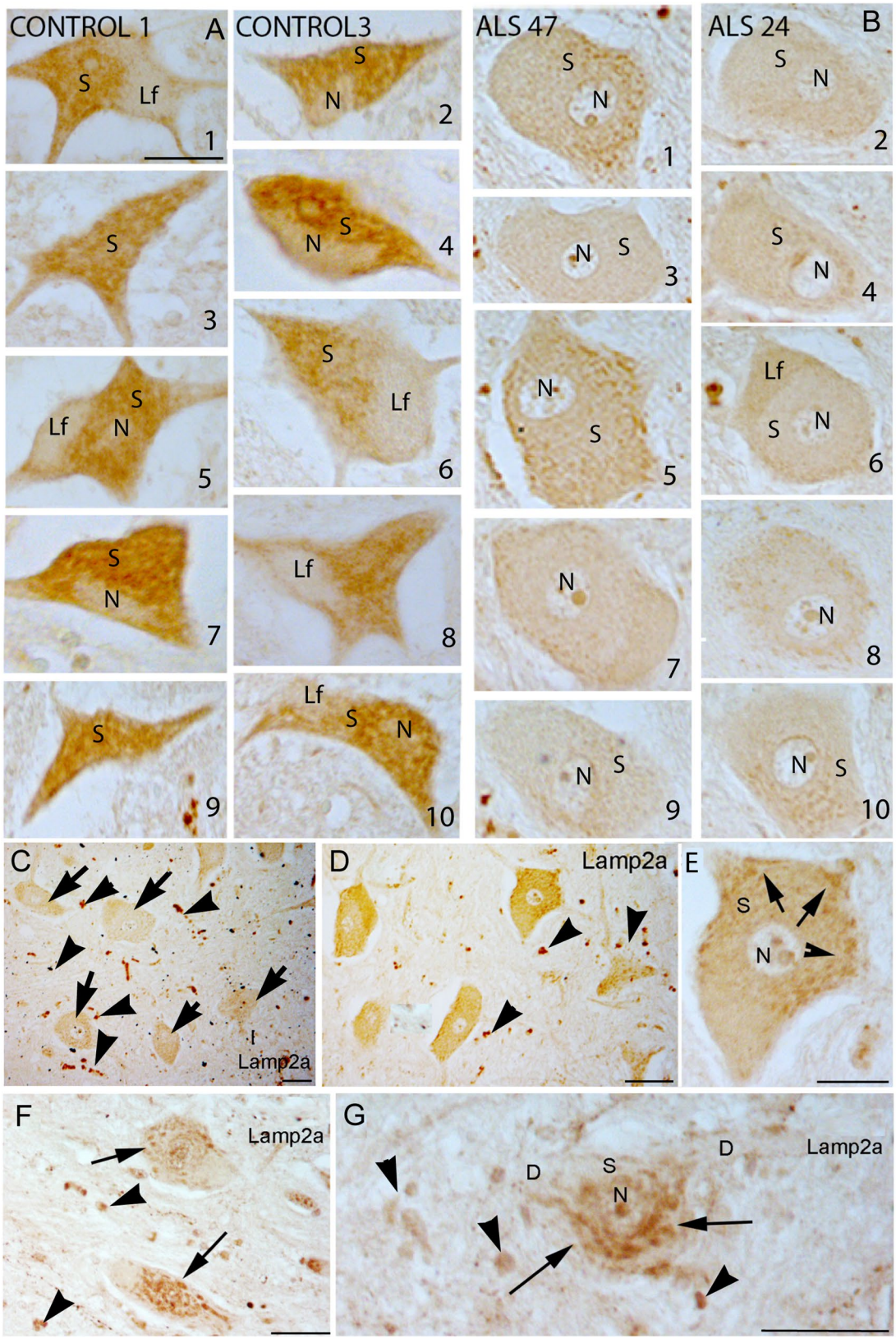

Fig. 2 (See legend on next page.)

(See figure on previous page.)

Fig. 2 Expression of LAMP2A in healthy and sALS motor neurons (MNs). **a** Ten MNs representing spinal motor neurons from two control spinal cords, showing high expression of LAMP2A in the perinuclear region (Control 1: cells 1, 3, 5, 7, and 9; Control 3: cells 2, 4, 6, 8, and 10). **b** Ten distinct spinal MNs from two different sALS spinal cords, displaying low expression of LAMP2A (ALS 47: cells 1, 3, 5, 7, and 9; ALS24: cells 2, 4, 6, 8, and 10). **c**–**d** Low-magnification images showing weak LAMP2A expression in MNs (arrows) and strong LAMP2A expression in glial cells (arrowheads) within the anterior gray horn. **e** In some sALS MNs, LAMP2A-positive puncta are localized at the periphery of the cytoplasm (arrows). **f**–**g** Images of MNs in sALS spinal cords exhibit nearly normal localization of LAMP2A-positive puncta (arrows), along with strong LAMP2A expression in glial cells (arrowheads). Abbreviations: S = Neuronal soma; N = Neuronal nucleus. Scale bar: A, B, C: 60 µm; D: 60 µm; E: 30 µm; F, G: 60 µm

reduced expression of LAMP2A (Figs. 2a and b and 3a–e), a small subset (approximately 5–10% of MNs) exhibited peripheral or normal cytoplasmic distribution of LAMP2A-positive puncta (Fig. 2d, e). These results were corroborated by quantitative immunofluorescence analysis of LAMP2A expression. Analysis of 40 motor neurons (MNs) from four control spinal cords and 50 MNs from five sALS patients revealed a significant reduction in LAMP2A expression in sALS MNs compared with controls (Fig. 3v), consistent with reduced chaperone-mediated autophagy (CMA) activity. These findings suggest a decrease in CMA activity in sALS MNs relative to controls. In contrast, spinal MNs from the patient ALS40 displayed a moderate reduction in LAMP2A expression in approximately 60% of MNs (Fig. 2f, g; Supplementary Fig. 5).

Macroautophagy is preserved in sALS patients' motor neurons

In animal models of ALS, impaired MA and autophagosome formation have been reported [9, 19, 24, 32, 33, 74]. Therefore, to evaluate MA function in our human SC sections, we examined the expression of the autophagosome marker microtubule-associated protein light chain 3 (LC3) using immunohistochemistry [39]. Moreover, in selective MA, a specific interaction between p62 and LC3 is necessary to mediate the autophagic degradation of p62-positive structures [92]. The detection of p62-positive aggregates serves as an indicator of MA deficiency in tissues [92]. Consequently, p62 expression was also analyzed in our samples. Lastly, to investigate lysosomal formation and distribution in MNs we assessed the expression of the lysosomal enzyme glucocerebrosidase (GBA) [8].

Abundant immunopositive LC3 puncta aggregates were detected in the cytoplasm of both controls (Fig. 3f) and sALS spinal MNs (Fig. 3g-j). GBA immunolabeling was observed as a puncta pattern dispersed in the cytoplasm with higher perinuclear density (Fig. 3k-p).

To compare CMA, MA and lysosomal formation, we quantified immunopositive puncta of LAMP2A, LC3B, and GBA in SC MNs where the nucleus was clearly detected and in nonconsecutive sections to ensure that we did not count the same neuron multiple times. We selected 10 MNs of the antero-lateral MNs column in two control SC (Controls 1 and 3; 5 MNs at cervical and 5 MNs at lumbar segments), as well as 10 MNs of antero-lateral MNs column in two patients' SC, ALS 24 and 47 (5 MNs at cervical and 5 MNs at lumbar segments) (Fig. 3a-p). Our quantitative analysis demonstrated that LAMP2A expression is significantly reduced in sALS MNs, while autophagosomes formation detected by LC3 puncta and the number of lysosomes related to the GBA expression showed no significant differences (Fig. 3q). Furthermore, to confirm the specificity of the increased LAMP2A immunoreactivity in control SC MNs, we observed no qualitative differences in LC3 expression between MNs and TCN in control samples (Fig. 3r, s).

The analysis of P62-protein intracytoplasmic deposits in all the parallel series processed by P62 immunohistochemistry detected only 5 MNs in lumbar sections of ALS 40 patient SC (Fig. 3t), where also TDP-43 deposits appeared in the parallel series (Fig. 3u). All other control and sALS SC samples showed no p62 deposits. These results further support that MA is not significantly affected in human sALS MNs.

Analysis of LAMP2A, LC3, GBA, and p62 expression in MNs from control and ALS patient samples did not reveal any significant sex- or age-related differences in expression levels. However, in ALS 40, increased LAMP2A expression (Supplementary Fig. 5) and p62 accumulation (Fig. 3t) were observed in a subset of MNs, suggesting the possibility of a distinct etiological variant of sALS in this patient.

Glial cells increase the expression of LAMP2A in sALS spinal cords

In control SC tissue, glial cells in both white and gray matter exhibit weak LAMP2A expression (Fig. 4a; Supplementary Fig. 3d, f, g). In contrast, LAMP2A-immunopositive glial cells of sALS SC were observed in the anterior horn gray matter and were more abundant in the lateral and medial corticospinal tracts (lcst and mcst; Fig. 4b–c). High-magnification images of the lcst revealed intensely LAMP2A-expressing cells with reactive astroglial morphology [40, 85], interspersed among LAMP2A-negative axonal fascicles (Fig. 4d–f). GFAP immunostaining highlighted the typical morphology of reactive astrocytes (Supplementary Fig. 4a–c), which in some cases displayed disrupted cytoplasmic processes and somatic vacuolization (Supplementary Fig. 4c). This phenomenon, known as clasmatodendrosis [88], was first described by Ramón y Cajal in 1913 [17].

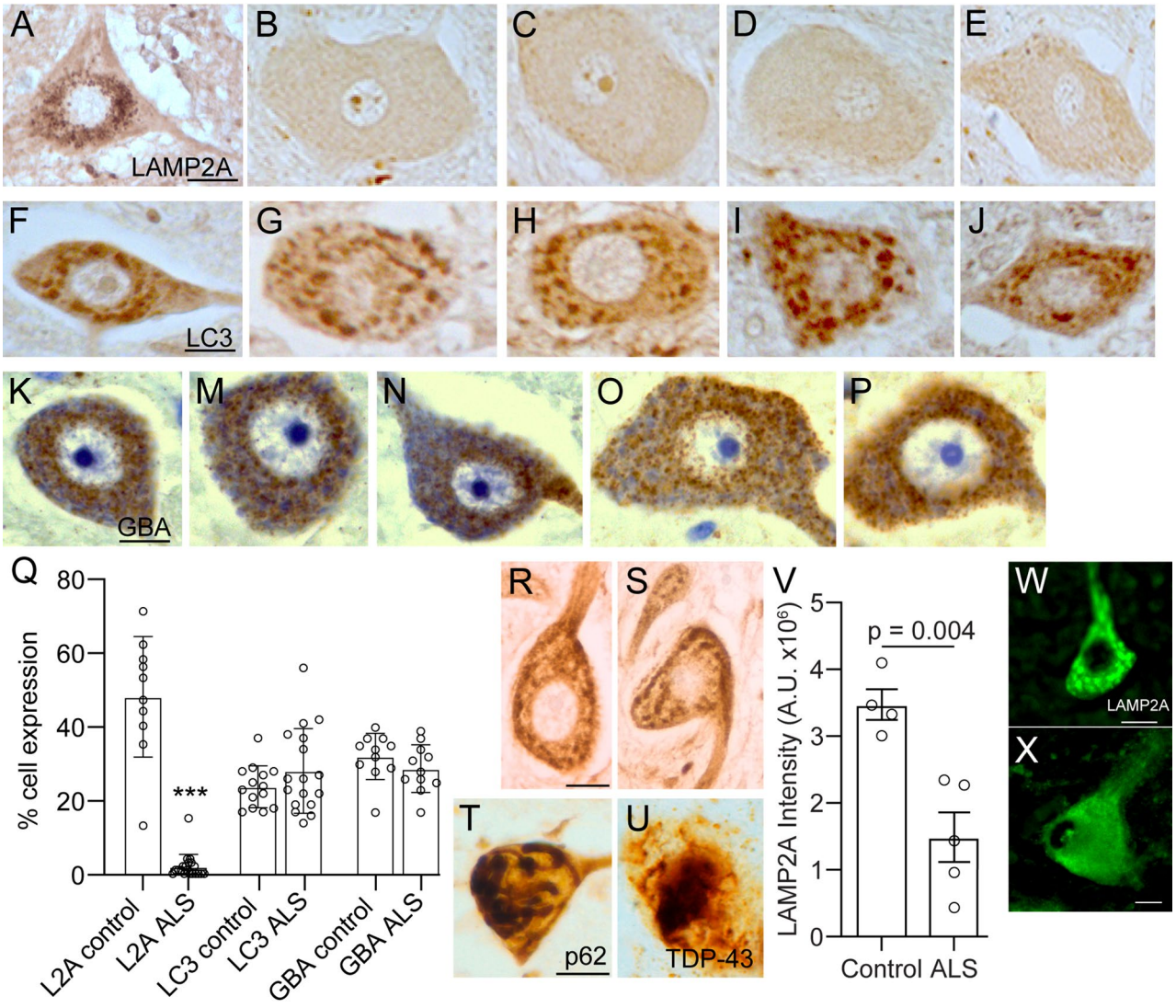

Fig. 3 Differential expression of LAMP2A, LC3 and GBA markers in control and sALS spinal MNs. **a**-**e** Presence of perinuclear expression of LAMP2A in control MNs (A) but not in sALS **b**-**e**. **f**-**j** Autophagosomes detected by LC3 puncta aggregates are present in both control (f) and sALS neurons **g**-**j**. **k**-**p** GBA positive neurons show elevated perinuclear density in control (k) and sALS neurons **m**-**p**. **q** LAMP2A expression is significantly reduced in sALS MNs (***$p < 0.001$) while remaining unaltered in LC3 and GBA positive cells. **r**-**s** Microphotographs showing LC3 expression in thoracic column neurons of sALS spinal cord. **t**-**u** Localization of p62 (t) and TDP-43 (u) deposits in sALS lumbar spinal MNs. (v) Quantification of LAMP2A fluorescence intensity (CTCF, A.U. x106) in control and sALS MNs. Each point represents the mean value of an individual subject ($n = 4$ Controls, $n = 5$ sALS; 10 MNs per subject). Data are shown as mean ± SEM; **$p = 0.004$ (unpaired t-test). (w, x) Representative immunofluorescence images of LAMP2A (green) in Control (W) and sALS (X) motoneurons. Scale bar: (a-p) 40 µm; r,s: 40 µm; t, u: 40 µm; w, x: 20 µm

To determine if this increase of LAMP2A is due to the inflammation associated with the axonal neurodegeneration resulting from degeneration of primary cortical MNs, we studied the presence of immunocompetent cells infiltration using IBA1 and CD68 immunohistochemistry. LAMP2A expression in astroglial cells was colocalized within lcst and mcst, alongside IBA1-positive microglia (Supplementary Fig. 4d-f). There was also a notable infiltration of CD68-immunopositive cells, which appeared to be concentrated within perivascular spaces (Fig. 4g, h; Supplementary Fig. 4d, e). IBA1-positive microglial cells were also observed surrounding axons within these tracts (Supplementary Fig. 4f). Therefore, the significant increase of LAMP2A expression in glial cells may be due to an inflammatory process in corticospinal tracts as a consequence of axonal degeneration. Moreover, high-power pictures from the anterior horn showed the presence of CD68 immunopositive cells between MNs (Fig. 4i), suggesting that an inflammatory process in the gray matter may also be associated with a reactive increase of LAMP2A expression in some glial cells. Double immunodetection using LAMP2A and IBA1 showed the distribution of LAMP2A-positive

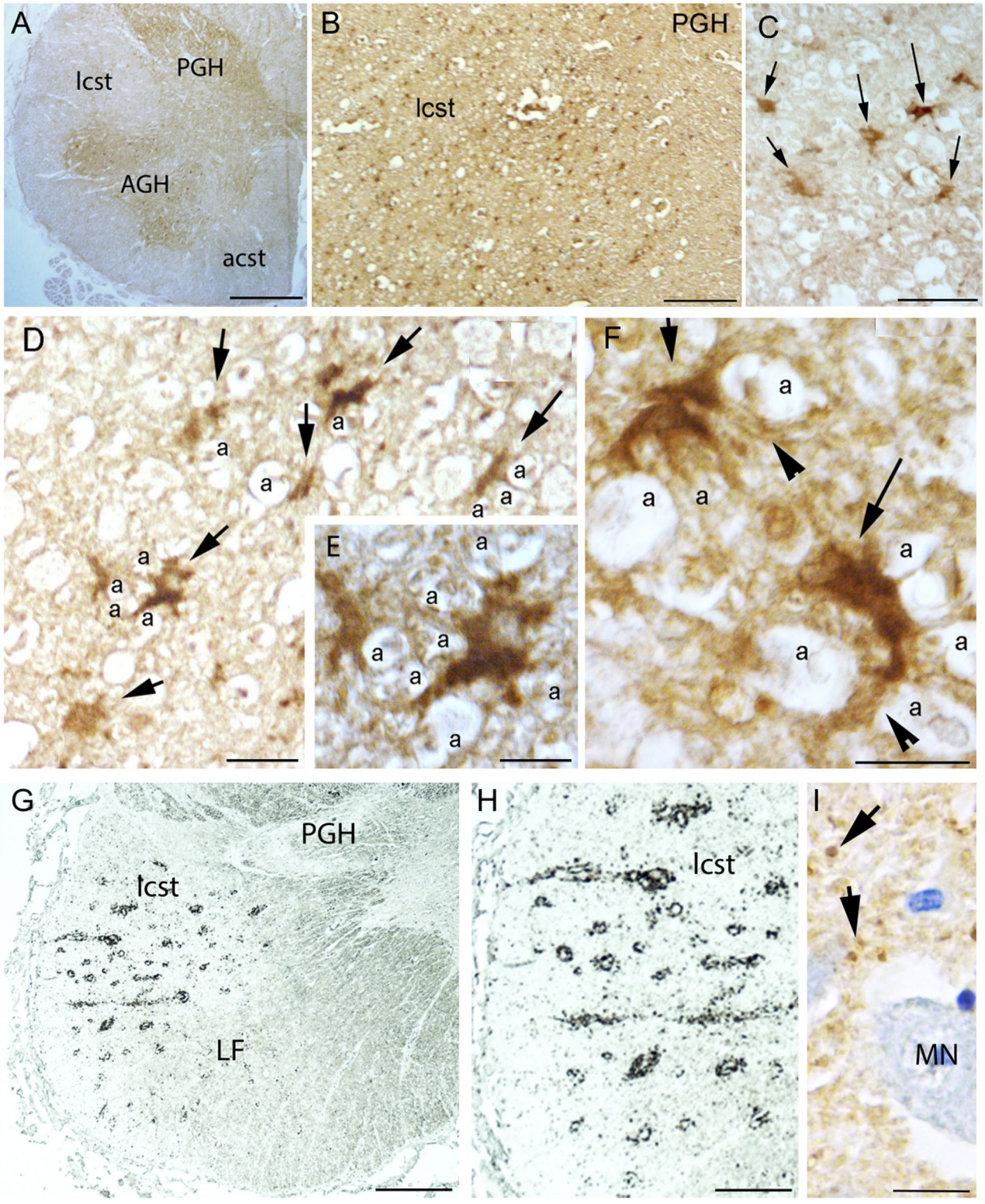

Fig. 4 LAMP2A and CD68 inflammation marker expression in glial cells. **a** Control spinal cord section showing the absence of LAMP2A immunolocalization in the white matter. **b**-**f** LAMP2A positive astroglial cells in the lateral corticospinal tract of sALS spinal cord sections (arrows). Corticospinal axonal profiles are identified (a). Some LAMP2A positive glial cells showed cellular processes evolving axonal profiles (f, arrowheads). **g**, **h** CD68 expression as a marker for inflammatory cells. Perivascular infiltration of CD68 positive cells is predominant in the lateral corticospinal tract. **i** Inflammatory cells (CD68 immunopositive) are also detected in the anterior gray matter (arrows). LF: Lateral funiculus; MN: Motoneuron; PGH = Posterior gray horn. a = axon. Scale bars: a: 3 mm; b: 2 mm; c: 150 µm; d: 60 µm; e: 30 µm; f: 30 µm. g: 2 mm; h: 200 µm; i: 30 µm

astroglia and IBA1-positive microglia in the cortico-spinal tracts (Supplementary Fig. 4f).

The analysis of glial activation by LAMP2A expression in lateral and medial cortico-spinal tracts of sALS MNs did not show any age- or sex-specific differences when comparing expression levels in SC sections.

TDP-43 proteinopathy in LAMP2A deficient sALS motoneurons.

Spinal MNs from control SC exhibited TDP-43 immunoexpression primarily in the cell nucleus (Fig. 5). We performed ChAT (Fig. 5a) and double ChAT/TDP-43 immunohistochemistry (Fig. 5b, c), identifying colocalization of TDP-43 nuclear expression in ChAT-positive MNs (Fig. 5b, c). Additionally, we conducted double immunohistochemistry in another section series to investigate the localization of TDP-43 and LAMP2A

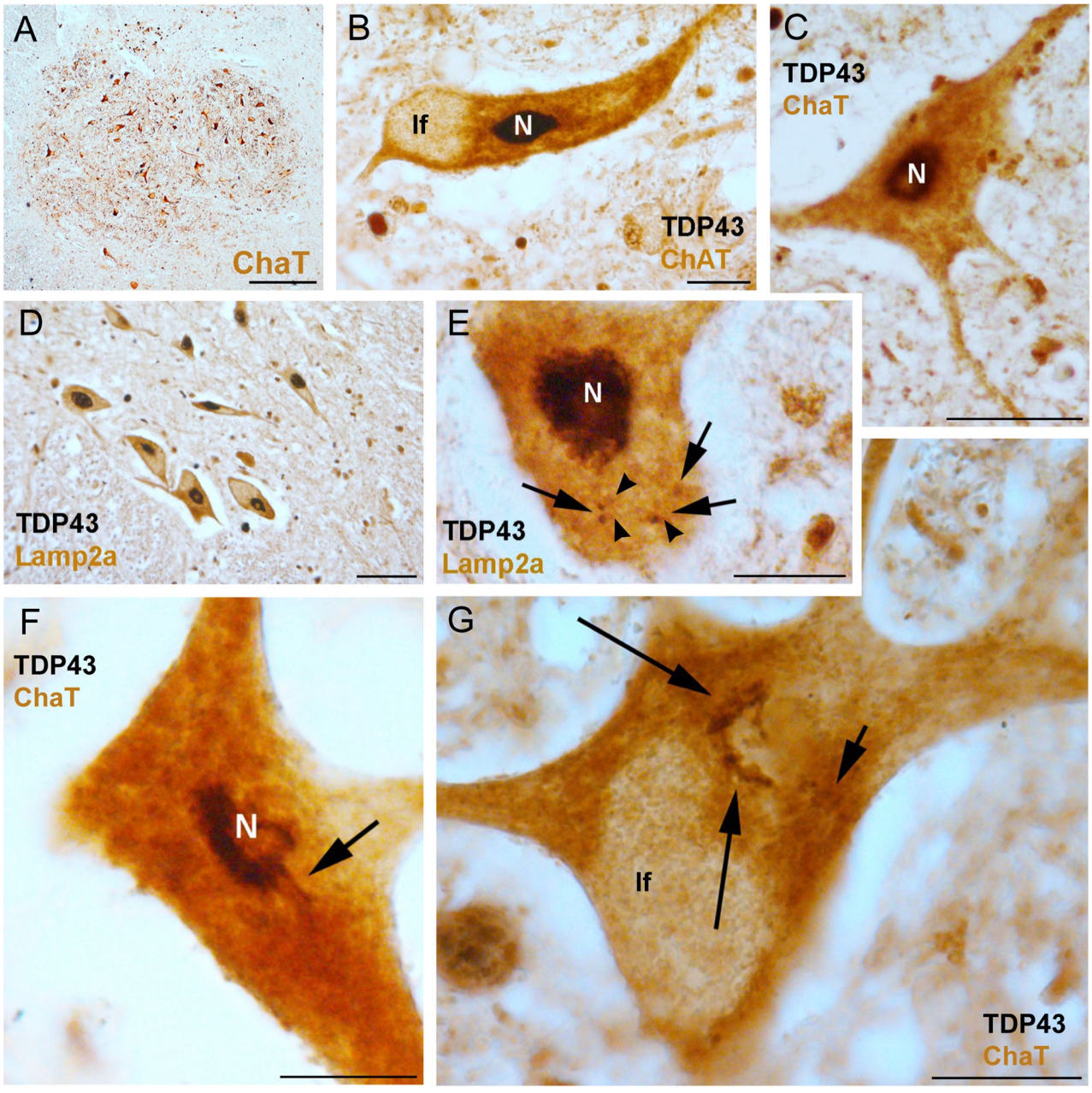

Fig. 5 Co-expression of LAMP2A and TDP-43 protein in healthy neurons. **a** ChAT positive neurons in the AGH specifically identify MNs. **b**, **c** Co-expression of TDP-43 protein predominantly in the nucleus (black staining) and ChAT protein in the cytoplasm (brown staining). **d**, **e** Co-expression of LAMP2A (brown staining) and TDP-43 (black staining), showing the close cytoplasmic colocalization of TDP-43 (**e**, big arrows labelling black punctata) and LAMP2A positive zones (**e**, small arrows labelling brown punctata) (arrows). **f**, **g** Co-expression of ChAT (brown staining) and TDP-43 (black staining). Arrow in **f** identifies nucleo-cytoplasmic connection of TDP-43 protein. **g** Cytoplasmic colocalization of TDP-43 (large arrows) and ChAT (small arrows) positive zones. Lf = Lipofuscin. N: nucleus. Scale bars: a: 600 µm; b: 30 µm; c: 60 µm; d, f: 50 µm; g: 30 µm

in spinal MNs (Fig. 5d-g). Some TDP-43 immunopositive puncta were detected in the cytoplasm (Fig. 5e), occasionally in continuity with its nuclear expression (Fig. 5f), suggesting a nucleo-cytoplasmic transfer of this protein [5]. These cytoplasmic TDP-43-positive colocalized with LAMP2A-positive puncta (Fig. 5d, e). The observed colocalization of TDP-43 and LAMP2A in the cytoplasm of control MNs further supports the involvement of CMA in TDP-43 cytoplasmic clearance.

Nuclear depletion and cytoplasmic deposits of TDP-43 in motor system neurons and glia have been described in ALS patients and animal models [18, 23]. As mentioned before, it has also been reported that TDP-43 is a substrate of CMA [37, 44, 55, 66]. Therefore, we explored if LAMP2A deficient MNs of our sALS patients presented TDP-43 proteinopathy. We performed TDP-43 immunohistochemistry on sections of parallel series as described previously: C3-4, T8-9, L3-4, and S2-3 SC segments (n = 10 slides in each segment) of sALS patients SC (n = 10; see Supplementary Table 1). Anti-TDP-43 immunohistochemistry was counterstained with Cresyl violet, showing different degrees of proteinopathy in sALS spinal MNs. Most MNs in the spinal anterior gray matter showed TDP-43 proteinopathy (90–95% of MNs) (Fig. 6a-g, k). We classified TDP-43 cytoplasmic inclusions according to Kon et al. [50] into three categories: (1) fine punctate granules scattered diffusely in the cytoplasm (DPSC) (Fig. 6k), (2) round inclusions (RIs) about 1–15 μm in diameter (Fig. 7a, b), and (3) skein-like inclusions (SLIs) (Fig. 6d-f). Predominant nuclear immunolocalization and punctate granules in the cytoplasm, similar to those observed in control MNs, were observed in 3–5% of sALS MNs (Fig. 6, i). Additionally, 30–35% of MNs showed only partial or total depletion of nuclear TDP-43 immunopositive granules, with DPSC (Figs. 6-k), but without important cytoplasmic deposits, which has been described as the initial proteinopathy in relation to stress granules in ALS MNs [50, 62]. In the rest of the analyzed MNs (60%), they showed nuclear clearance accompanied by cytoplasmic deposits, together with strong degenerative cytoplasmic vacuolization in colocalization with TDP-43 aggregates, in agreement with Martin [59] (Fig. 6-g). Moreover, the normal cisternal pattern of Nissl bodies in the cytoplasm (Fig. 6-j) disappeared in sALS MNs showing TDP-43 aggregates and was replaced by a granular, scattered pattern intermixed with DPSC of TDP-43 (Fig. 6, g, k). In contrast, anterior horn interneurons showed normal nuclear TDP-43 expression (Fig. 6m).

To analyze the co-expression of TDP-43 and LAMP2A in the patient's MNs, another parallel series of sections were processed by double immunohistochemistry using anti-TDP-43 and anti-LAMP2A antibodies (Fig. 7). First, the reduction of LAMP2A expression in sALS MNs was clear, being especially evident in MNs with RIs (Fig. 7, b). Second, in most sALS MNs with reduction of LAMP2A expression, nuclear clearance and DPSC of TDP-43 was clearly detected (Fig. 7). In addition, the distribution and typology of TDP-43 aggregates in LAMP2A-depleted MNs were heterogeneous and sometimes combined in the same cell, detecting a mixture of DPSC with round aggregates and SLIs. TDP-43 filiform inclusions were localized into MNs dendritic proximal segments (Fig. 7, f, i, j). Moreover, some MNs showed TDP-43 filaments across the cellular membrane (Fig. 7, g, h). While we cannot exclude the possibility that these transmembrane localization of TDP-43 filaments may result from fixation artefacts, the presence of TDP-43 filaments in the interstitial space near MNs (Fig. 7j, k), suggest the possibility of transmembrane trafficking and raises the potential for transcellular transmission of misfolded TDP-43 protein.

Interestingly, ALS40 SC MNs showed a reduced degree of TDP-43 proteinopathy. Actually, although more than 40% of MNs showed TDP-43 cytoplasm aggregates (Supplementary Fig. 5, a-c), more than 30% of MNs showed only nuclear depletion of TDP-43, and another 30% normal localization of this protein (Supplementary Fig. 5). These findings suggest that CMA is more active in this patient, as described previously (Fig. 2, g). Accordingly, we examined the expression of LAMP2A in ALS40 SC (Supplementary Fig. 5, h). Our analysis revealed that the ALS 40 SC MNs exhibited higher LAMP2A expression than the other sALS SC, which may account for the reduced TDP-43 pathology. Quantification of LAMP2A expression in ALS40 SC MNs was similar to control SC MNs (Supplementary Fig. 5).

The analysis of TDP-43 expression, and TDP-43/LAMP2A co-expression in sALS MNs, with the exception of ALS40, did not show any sex-specific differences when comparing expression levels in sections from SC (Supplementary Table 1). As was described above, ALS40, although with more LAMP2A expression and less degree of TDP-43 proteinopathy, has the faster evolution: 11 months in comparison to the rest with a mean of 27,4 months (Supplementary Table 1). This may suggest a different pathogenic mechanism underlying the MN degeneration and reflects the heterogeneity of the disease evolution in each patient.

Onuf's nucleus motoneurons exhibit high expression levels of LAMP2A in sALS spinal cords.

In the sacral levels of sALS patients, Onuf's nucleus was identified due to the presence of a significant number of ChAT-positive MNs in the anterior horn, between anterolateral and anteromedial columns (Fig. 8a-c). While surrounding spinal MNs in the anterior horn showed a cytoplasm with a degenerative vacuolar profile, Onuf's MNs appeared without cytoplasmic pathology (Fig. 8, c, h). Moreover, Onuf's MNs exhibited strong LAMP2A expression, with punctate lysosomal immunoreactivity

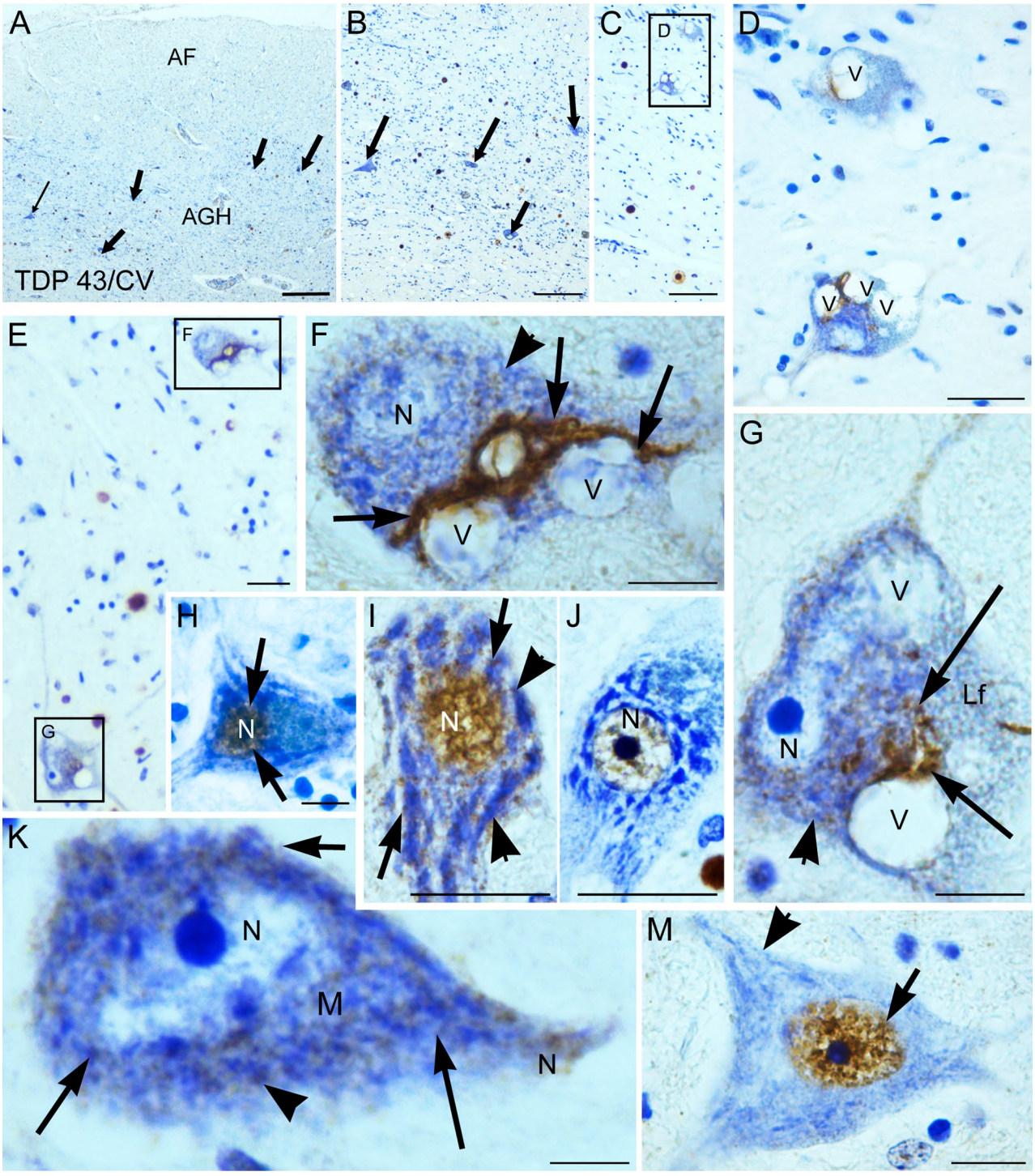

Fig. 6 TDP-43 immunostaining in sALS MNs shows proteinopathy as nuclear clearance and cytoplasmic deposits. **a**-**c** MNs in the AGH are identified by their large size in Nissl's staining. Most of the MNs showed nuclear clearance and TDP-43 cytoplasmic aggregates and large vacuoles in their cytoplasm (arrows). **d** High power image of two MNs identified in c, showing large cytoplasmic vacuoles in contact with TDP deposits, **e**-**g** Images of MNs in sALS spinal cord to illustrate nuclear clearance and TDP-43 aggregates (arrows) in close contact with cytoplasmic vacuoles. **f**, **g** The cisternal pattern of Nissl bodies in the cytoplasm exhibits a scattered granular pattern (arrowheads). **h** MN showing nuclear localization of TDP-43. **i** MN displaying normal nuclear localization of TDP-43 in the nucleus and fine punctate granules scattered diffusely in the cytoplasm (arrows) with normal cisternal pattern of Nissl bodies (arrowheads). **j** MN showing normal localization of TDP-43 in the nucleus without cytoplasmic deposits. **k** MNs showing only TDP-43 nuclear clearance, with TDP-43 cytoplasmic punctate aggregates (arrows) also exhibited Nissl cistern distortion (arrowheads). **m** Interneurons in the AGH show nuclear localization of TDP-43 (arrow) and normal pattern of Nissl cisterns (arrowheads). AF = Anterior Fasciculus. AGH = Anterior gray horn. CV = Cresyl violet. N = nucleus. V = Vacuoles. Scale bars: a: 600 µm; b, c: 350 µm; d, e: 80 µm; f, g, h: 20 µm; i, j: 30 µm; k: 15 µm; m: 20 µm

Figure 7

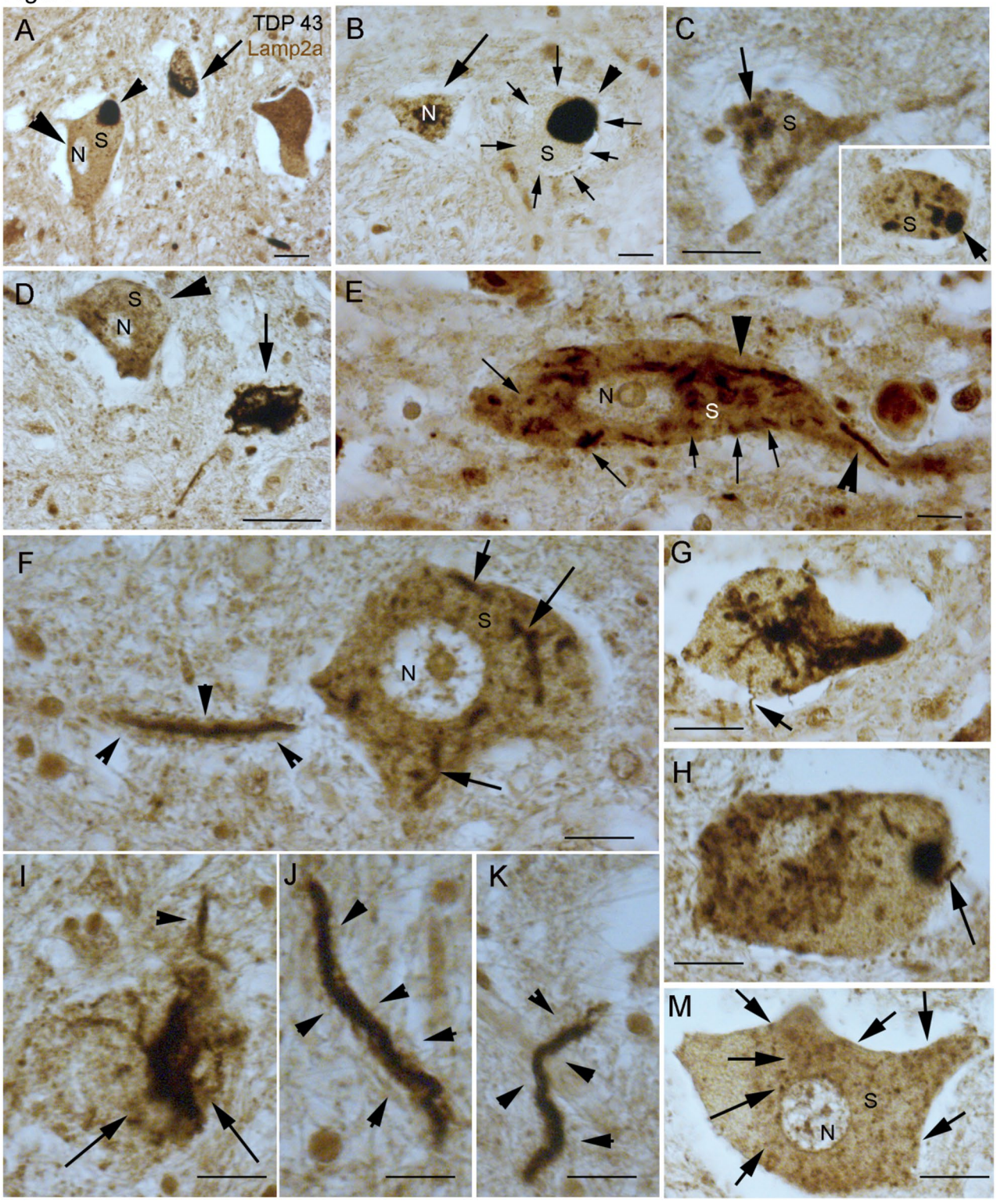

Fig. 7 (See legend on next page.)

(See figure on previous page.)

Fig. 7 Co-expression of TDP-43 and LAMP2A shows nuclear clearance and aberrant cytoplasmic deposits of TDP-43, together with low LAMP2A expression. **a** sALS MNs showing TDP-43 nuclear clearance (large arrowhead), round inclusions (RIs) (small arrowhead) and skein-like inclusions (SLIs) (arrow) in their cytoplasms, with very low LAMP2A expression. **b** sALS MN showing TDP-43 round inclusions (RIs) (arrowhead) with very low LAMP2A expression in the cytoplasm (small arrows); interneurons (large arrow) show normal nuclear localization of TDP-43, with some punctate expression in the cytoplasm. **c** RLIs in the cytoplasm of MNs (arrows) and weak expression of LAMP2A. **d** Nuclear clearance and fine punctate granules scattered diffusely in the cytoplasm (DPSC) (arrowhead) and SLIs in another MN (arrow). **e** sALS MN showing RLIs (arrows) and filiform aggregates in the soma and dendrites of MNs (arrowhead). **f** sALS MN showing filiform aggregates in the soma (arrows) and dendrites (arrowheads). **g**, **h** MNs showing RLIs, SLIs TDP-43 inclusions and filiform aggregates across the cellular membrane (arrows). **i** sALS MN showing SLIs in the soma (arrow) and filiform aggregates in the dendrites (arrowhead). **j** TDP-43 filiform aggregate into a dendrite (arrowheads). **k** TDP-43 filiform aggregate in the interstitial space (arrowhead). **m** sALS MN showing nuclear clearance and DPSC (arrows). N = Nucleus. S = Soma. Scale bars: a: 60 µm; b: 40 µm; c, d: 60 µm; e: 40 µm; f: 25 µm; g, h, i: 30 µm; j, k: 15 µm; m: 40 µm

comparable to that of control SC MNs (Fig. 8d). In contrast, spinal MNs in the same segment showed markedly reduced LAMP2A expression, with sparse puncta predominantly localized at the cell periphery (Fig. 8e).

We have studied the localization of TDP-43 protein in Onuf's MNs of sALS patients in combination with LAMP2A expression or Nissl staining. In Onuf's MNs, TDP-43 was predominantly localized in the nucleus of LAMP2A-positive MNs, similar to control MNs (Fig. 8, g), and the normal cisternal pattern of Nissl bodies in the cytoplasm was detected (Fig. 8, i). These findings support that high CMA activity is crucial to maintain Onuf's MNs alive in sALS patients and reinforces the possibility that CMA in SC MNs may play a role in preventing TDP-43 proteinopathy and MNs vulnerability of sALS.

Discussion

Our results show for the first time that human SC MNs exhibit high levels of LAMP2A expression, suggesting that MNs require increased CMA activity to function properly. Interestingly, CMA activity regulates neuronal activity in excitatory neurons and CMA reduction levels are associated with synaptic alteration in a mouse model of Alzheimer [46]. On the other hand, SC samples from sALS patients showed reduced LAMP2A expression in their MNs. These findings may explain the selective vulnerability of MNs observed in prior studies, which has been attributed to structural and functional differences unique to MNs [65, 67, 83]. Neuronal hyperexcitability caused by reduced CMA, associated with synaptic protein dysregulation, reversed by CMA restoration in an Alzheimer's disease mouse model [46], underscores a potential key role for CMA in regulating MNs excitability. These findings, together with selective increases of LAMP2A expression in MNS, implicate CMA dysfunction–driven excitotoxicity as a potential mechanism contributing to MNs degeneration in ALS. Despite the reduced LAMP2A expression in sALS MNs, MA appeared unaffected compared to control MNs, as evidenced by the presence of autophagosomes detected by robust LC3B-positive cytoplasmic puncta pattern. GBA expression was unchanged, indicating normal lysosomal activity, including autophagosomes. TDP-43 was primarily localized in the nucleus of control spinal MNs, but in sALS MNs, it was absent from the nucleus and accumulated in the cytoplasm. Notably, Onuf's nucleus in sALS patients showed higher LAMP2A expression and protection from TDP-43 cytoplasmic pathology. Finally, ALS40-specific differences further support the role of LAMP2A activation in preventing or delaying TDP-43 proteinopathy in sALS patients, also highlighting the heterogeneity of the etiology and pathology of this disease.

CMA is selectively upregulated in spinal cord MNs

CMA is a selective autophagic pathway that targets proteins with a lysosomal targeting motif, such as the pentapeptide chain KFERQ [48]. The chaperone Hsc70 binds to KFERQ-containing proteins, transporting them to the lysosomal surface, where they interact with LAMP2A before being unfolded and degraded in the lumen. CMA degrades approximately 30–35% of cytosolic proteins, impacting critical processes such as lipid and glucose metabolism, DNA repair, cellular reprogramming, stress responses, and immunological function [48, 53]. Impairment of CMA has been associated with several age-related diseases, including neurodegenerative disorders, atherosclerosis, metabolic diseases, and cancer [20, 24, 26, 27, 53, 57].

The elevated CMA activity in spinal MNs could be attributed to their large size and high firing rates, consistent with Henneman's size principle, which states that the size of a neuron is a crucial determinant in reaching the threshold for action potential firing [35]. Fast-fatigable motor units are more vulnerable to ALS, whereas slow motor units, which are more resistant, may help to reinnervate motor endplates [65, 67]. These findings suggest that the functional properties of MNs may influence their vulnerability to ALS. This functional activity necessitates the regulation of ion channels, receptor proteins, and ion buffering mechanisms, all of which contribute to the need for enhanced proteostasis control. Additionally, due to their highly polarized nature MNs require efficient protein production and degradation pathways to survive. As mentioned earlier, CMA has been implicated in synaptic plasticity of excitatory neurons [46], and, therefore, in neurodegenerative diseases, contributing to the degradation of pathogenic proteins such as α-synuclein and tau [13, 16, 21, 24, 29, 36, 53]. Loss of CMA function leads to

Figure 8

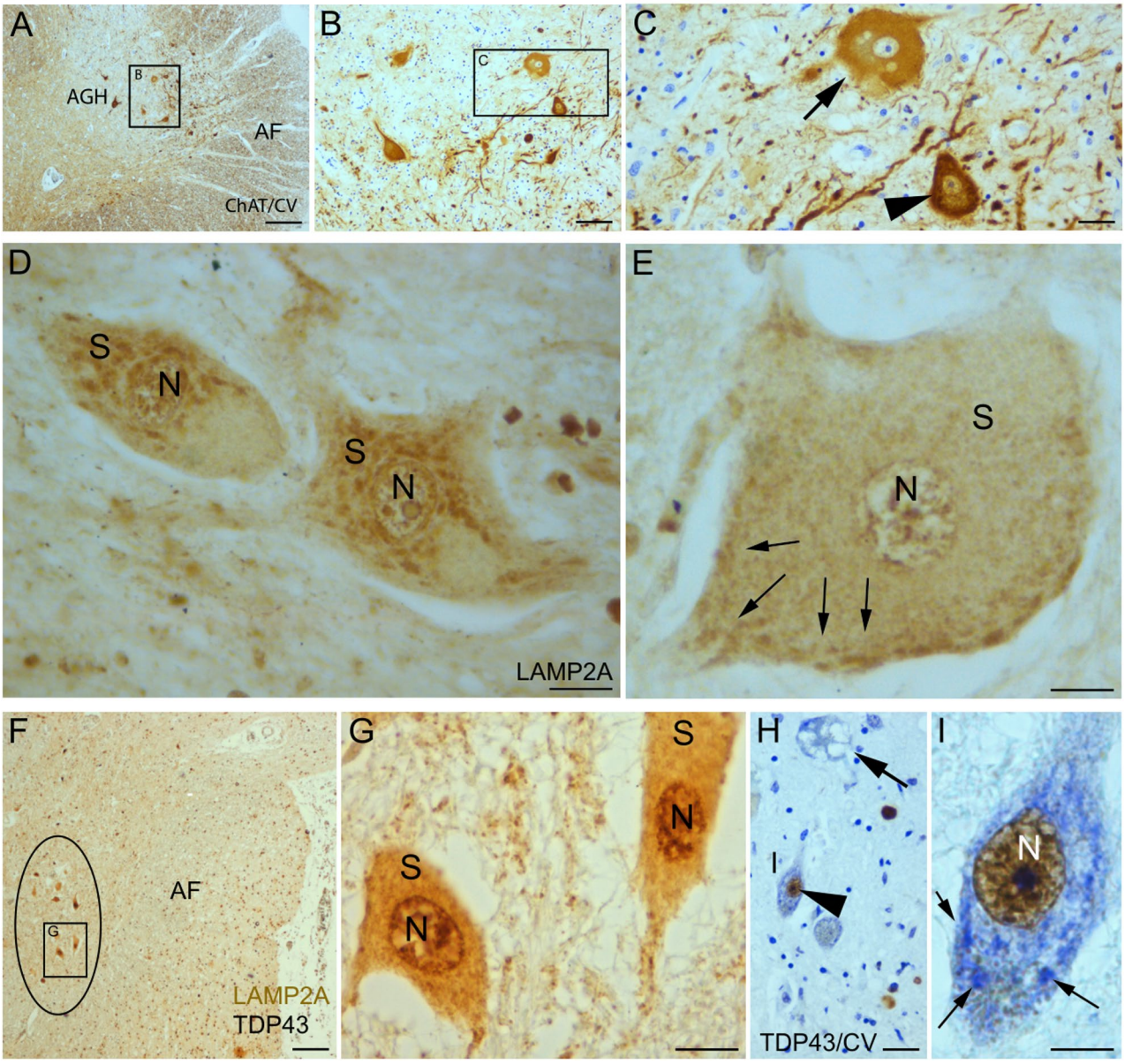

Fig. 8 Detection of Onuf's nucleus through ChAT immunostaining and its co-expression of LAMP2A and TDP-43. **a**-**c** ChAT positive MNs with cresyl violet counterstaining. **b**, **c** High power microphotograph showing an ChAT positive spinal MN with cytoplasmic vacuolization (arrow) and an Onuf`s ChAT positive MN without structural pathology. **d** High expression of LAMP2A in sALS Onuf's MNs. **e** Spinal MNs close to Onuf's MNs showed low and predominantly peripheral expression of LAMP2A (arrows). **f**, **g** Nuclear localization of TDP-43 in Onuf's MNs showing LAMP2A highly expressed in the MNs perinuclear somatic area. **H** Spinal MNs near to Onuf's MNs (arrowhead) show cytoplasmic vacuolization (arrow). **I** Nissl bodies' staining with cresyl violet and TDP-43 immunostaining in sALS Onuf's MNs, showing normal cisternal structures (arrows). AGH = Anterior gray horn. AF = Anterior funiculus. N = Nucleus. S = Soma. Scale bars: a: 300 µm; b: 150 µm; c: 70 µm; d: 40 µm; e: 30 µm; f: 200 µm; g: 70 µm; h: 60 µm; i: 40 µm

significant changes in the neuronal proteome, disrupting essential neuronal functions and promoting neurodegeneration [13, 77]. Moreover, the specificity of high requirements of CMA function in MNs could explain their heightened vulnerability to CMA impairment compared to other cell types, providing a potential mechanism for the selective neurodegeneration of MNs in sALS.

Interestingly, Khawaja et al. [47] reported that CMA activity declines with age across most organs and cell types, with a more marked reduction observed in males. This decline is often associated with a reduced number of lysosomes functionally competent for CMA, suggesting that sex-specific differences in CMA activity may influence tissue vulnerability to age-related degenerative processes. Jacob et al. [38] reviewed the mechanisms

underlying sexual dimorphism in ALS, emphasizing sex-specific heterogeneity in both genetic and non-genetic mechanisms across experimental models and patient cohorts. Within this framework, the apparent accelerated decline of CMA observed in males, reflected by LAMP2A expression levels comparable to those of females approximately ten years older, may underlie the sex-biased prevalence and distinct clinical phenotypes of ALS. While age- and sex-associated reductions in CMA have been reported in murine models, including different gender-specific synaptic alterations [46], further studies are required to validate these patterns in human SC MNs and the possibility of similar alterations in neuromuscular junctions. In the present study, the limited sample size precluded definitive conclusions regarding age- or sex-related differences in LAMP2A expression in SC MNs.

CMA is downregulated in sporadic ALS spinal MNs

Spinal cord sections from sALS patients demonstrated reduced LAMP2A expression in MNs; however, approximately 5–10% of MNs exhibited only a partial reduction in LAMP2A levels. This observation may reflect intrinsic heterogeneity in LAMP2A expression among MNs or indicate a progressive decline in its expression, potentially contributing to, or resulting from, the differential vulnerability of MN populations based on their functional and structural properties.(as reviewed in Ovsepian et al. [67]).

While MA has been well studied in ALS [24, 37, 78, 81, 84], CMA remains less explored. Our analysis revealed that LC3 expression was comparable between control and sALS spinal MNs, suggesting preserved MA function in sALS. Despite its importance in neuronal homeostasis, MA does not appear to have cell-specific requirements in MNs, as no substantial differences in LC3 expression were observed between control MNs and other spinal neurons. Although MA impairments have been reported in ALS models, our findings suggest its role in disease pathophysiology may be secondary, with experimental activation potentially mitigating TDP-43 proteinopathy rather than addressing a primary defect [24].

A study by Arosio et al. [3] reported TDP-43 proteinopathy with reduced levels of Hsc70 in lymphomonocytes of sALS patients without change in LAMP2A. In contrast, our results demonstrate reduced LAMP2A expression specifically in sALS MNs, reflecting fundamental differences in cellular expression and autophagy requirements across cell types.

Mutations in the *LAMP2* gene cause Danon disease, an X-linked lysosomal storage disorder characterized by cardio-myopathy and cognitive dysfunction. The pathological hallmark of this disease is the accumulation of glycogen and autophagic vacuoles in cardiac and skeletal muscles [28, 30]. The cognitive dysfunction seen in humans with Danon disease suggests a critical role of LAMP-2 in brain function [77]. These cognitive abnormalities are likely due to hippocampal dysfunction, associated with altered lysosomal activity, including the accumulation of p62-positive aggregates, autophagic vacuoles, and lipid storage within neurons. Notably, in agreement with our results, Rothaug et al. [77] reported that the absence of LAMP2 did not appear to affect MA in the brain cells under physiological or starvation conditions. In Danon disease MNs degeneration has not been observed [28, 30], which may be attributed to the cell-type-specific role of LAMP2B, the isoform mutated in Danon disease [51, 93], or to the limited lifespan of patients, which may preclude the manifestation of MN degeneration.

The selective accumulation of TDP-43 in CMA-deficient MNs, in the absence of other CMA substrate accumulation, may reflect the compensatory degradation of these proteins via alternative pathways, such as endosomal microautophagy (eMI), which has been shown to process KFERQ-like motif–containing proteins [48, 94]. Although we did not observe major alterations in macroautophagy or lysosomal distribution in MNs from patients with sALS, investigating the role of eMI in human MNs may help clarify the specificity of TDP-43 pathology in sALS.

Interestingly, LAMP2A levels were significantly higher in glial cells of sALS patients. The upregulation of LAMP2A in glial cells may be a reactive response to inflammatory processes occurring in the anterior horn and corticospinal tracts [71, 94]. Axonal degeneration is known to trigger inflammation and oxidative stress in glial cells, leading to activation of NFE2L2, which in turn increases LAMP2A expression and enhances CMA activity [69]. Indeed, this inducible regulation of LAMP2A, and consequently of CMA activity, by NFE2L2 (coding NRF2 antioxidant transcription factor) is not sufficient to overcome the low LAMP2A expression observed in sALS MNs, despite their elevated oxidative stress [14, 67, 75]. Bono et al. [12] reviewed the possible role of alterations of antioxidant response in ALS neurons and glia by the activation of KEAP1-NRF2 without conclusive information on the primary cause of ALS. Interestingly, increased autophagy was reported by Ryu et al., [79] underlining clasmatodendrosis as an autophagic death of astrocytes (reviewed in Balaban et al. [6]). Although Guise et al. [34] found no significant differences in LAMP2A expression between ALS and control MNs using laser-guided tissue dissection, our results suggest that it may be due to the inclusion of perineuronal astroglial fragments in the dissected samples, which exhibit strong LAMP2A activation and could mask the reduced LAMP2A in MNs.

This supports the notion that the alteration in LAMP2A expression in sALS MNs is a primary, constitutive, cell-autonomous defect.

CMA in onuf's nucleus MNs and selective vulnerability in sALS

Our results also provide evidence that Onuf's nucleus in sALS patients retains LAMP2A expression. Slow motor units are then more protected, and they reinnervate the end-plate left by faster, fatigable motor units after cell death [65, 67]. Interestingly, our work is the first to show that LAMP2A expression is not deficient in the Onuf's MNs of sALS patients. The mechanisms by which Onuf's nucleus remains spared in ALS and other neurodegenerative diseases, but impaired in others, remains unknown. Recently, RNA-seq analysis of mice Onuf's nucleus extracted by laser microdissection revealed that matrix metalloproteinase-9 (MMP9), an inflammatory biomarker that is highly expressed by ALS-affected spinal MNs, is not overexpressed in Onuf's neurons [41]. This MMP9 may represent a factor to reduce EN1 transference from interneurons to MNs, decreasing the paracrine neurotropism of this factor [52]. This, along with proper CMA functioning, could lead to protection of this nucleus against ALS-mediated cell death. The localization of EN1 in spinal and Onuf's MNs may shed some light on these mechanisms. The differential CMA activation likely contributes to the protective mechanisms underlying the selective preservation of Onuf's MNs in sALS. We propose that maintained CMA function in these MNs protects against excitatory activity, TDP-43 proteinopathy and subsequent cell death.

TDP-43 and autophagy in sALS

Our findings demonstrate colocalization of LAMP2A and TDP-43 in the cytoplasm of control MNs, suggesting that CMA may facilitate cytoplasmic TDP-43 clearance. This supports the hypothesis that CMA dysfunction contributes to TDP-43 proteinopathy in sALS MNs.

In TDP-43 proteinopathy, alterations in the localization and function of other proteins have been described, including ribonucleoprotein K. The binding of ribonucleoprotein K with Nrf2 transcript was associated with an impaired translation of Nrf2 mRNA, leading to an insufficient antioxidant response and motoneuron degeneration [63].

Wang et al. [89] and Barmada et al. [7] observed that stimulating autophagy by increasing LC3 levels in mouse neurons and human MNs derived from iPSCs improved TDP-43 clearance and reduced protein toxicity. However, TDP-43 aggregation may also result from defects in other protein degradation systems, such as CMA or the ubiquitin-proteasome system [25, 45]. Our data demonstrate that human sALS spinal MNs show no alterations in MA, indicating that MA dysfunction is not a primary pathological feature of sALS. Although alterations of genes promoting TDP-43 proteinopathy have been linked to dysregulation of MA in in vitro cells and animal models [19], our patients did not have a family history of ALS or showed *C9ORF72* genetic mutations (data from patient's clinical record), which could potentially underlie MA dysfunction. Moreover, it has described a mutual negative interaction between TDP-43 cytoplasmic aggregates and MA mechanisms [74]. Actually, Park et al. [70] reported a reduction in MA in yeast as a result of TDP-43-induced toxicity following its overexpression. These findings suggest a potential reciprocal inhibition between MA and TDP-43 proteinopathy that requires further investigation in human MNs.

Conclusion

Our study shows for the first time a high CMA activity in healthy human spinal motor neurons, as evidenced by elevated LAMP2A levels. However, sALS patients show a significant decrease in LAMP2A expression that correlates with cytoplasmic aggregates and the nuclear clearance of TDP-43. Notably, MA markers such as LC3 and the lysosomal enzyme GBA remain unchanged. CMA is preserved in Onuf's nucleus MNs. Enhanced LAMP2A expression in glial cells indicates a maintained antioxidant response in other brain cells. These findings strongly implicate CMA impairment as a key determinant of selective MN vulnerability in ALS. Collectively our results provide novel insights into pathological protein accumulation mechanisms and highlight CMA enhancement as a promising therapeutic strategy to restore proteostasis and prevent neurodegeneration in ALS.

Abbreviations

a	Axon
AF	Anterior funiculus
AGH	Anterior gray horn
ALS	Amyotrophic lateral sclerosis
ChAT	Choline acetyltransferase
CMA	Chaperone-mediated autophagy
CV	Cresyl violet
DPSC	Fine punctate granules scattered diffusely in the cytoplasm
fALS	Familiar amyotrophic lateral sclerosis
GBA	Lysosomal enzyme glucocerebrosidase
GCs	Glial cells
H&E	Hematoxylin-Eosin
LC3	Autophagosome marker microtubule-associated protein light chain 3
lcst	Lateral corticospinal trac.
LF	Lateral funiculus
Lf	Lipofuscin
MA	Macroautophagy
mcst	Medial corticospinal trac
MMP9	Matrix metalloproteinase-9
MNs	Motoneurons
MNBMc	Mononuclear bone marrow cells
MS	Microscopy slides.
N	Neuronal nucleus
PF	Posterior funiculus.
PGH	Posterior gray horn.

RIs	Round inclusions
S	Neuronal soma
sALS	Sporadic amyotrophic lateral sclerosis.
SC	Spinal cord
SLIs	Skein-like inclusions
SNs	Sensory neurons
TCNs	Clarke's thoracic column neurons
TDP-43	Trans-activation response DNA-binding protein
TS	Tissue slides.
V	Vacuoles

Supplementary Information

The online version contains supplementary material available at https://doi.org/10.1186/s40478-026-02238-6.

Supplementary Figure 1: Diagram of spinal cord processing. Transversal trimming and selection of 4 tissue slides (TS) in each spinal cord region (yellow) that were cut and mounted in 20 parallel series. Although all selected TS have been cut and mounted, only one TS has been represented in figure for each spinal cord segment.

Supplementary Figure 2: Control of immunostaining. (a, b) Microphotographs of sections processed in parallel without the primary anti-LAMP2A antibody. No cells in the section appear immunoreactive in (a). Using Nomarski interference contrast in (b), several MNs are visible in the area shown in (a). (d, e) Microphotographs of sections processed in parallel without the primary anti-TDP-43 antibody and counterstained with cresyl violet. The MNs show no immunolabeling in either the nucleus or the cytoplasm. (f, g) Microphotographs of sections processed in parallel without the primary antibodies anti-CD68 (f) and anti-GFAP (g). Cells in the lateral funiculus show no immunolabeling.

Supplementary Figure 3: LAMP2A comparative expression in control spinal cord. (a, b, c) Microphotographs of a control thoracic spinal cord section processed for LAMP2A immunodetection. (a) Low-magnification image showing the localization of gray and white matter regions in the spinal cord. (b, c, d) High LAMP2A expression is selectively observed in motoneurons (MN) of the anterior gray horn, while no significant expression of LAMP2A is observed in glial cells (d, f, g), thoracic column neurons (e), or sensory neurons of the posterior gray matter (f). (h) Astrocyte in the anterior gray matter counterstained with cresyl violet. Abbreviations: AF = Anterior funiculus; AGH = Anterior gray horn; GC = Glial cell; LCST = Lateral corticospinal tract; MN = Motoneuron; PF = Posterior funiculus; PGH = Posterior gray horn; N = Neuronal nucleus; SN = Sensory neuron; TC = Clarke's thoracic column. Scale bars: a: 3 mm; b, c: 30 µm; d: 70 µm; e: 20 µm; f: 20 µm; g: 10 µm; h: 6 µm.

Supplementary Figure 4: LAMP2A expression in glial and immune cells of sALS spinal cord. (a, b, c) GFAP immunoreactive reactive astrocytes showing in some cases disrupted cytoplasmic expansions and somatic vacuolization (clasmatodendrosis; c). (d-f) IBA1 positive microglia (black staining) showed strong expression of LAMP2A (brown staining; large arrows) near to the LAMP2A positive perivascular immune cells (small arrows) and astrocytes (arrowheads) in the lateral corticospinal tract. Scale bars: a-c: 20 µm; d: 50 µm; e: 50 µm; f: 40 µm.

Supplementary Figure 5: LAMP2A expression in sALS MNs with low TDP-43 proteinopathy (ALS40). (a, b) Microphotographs of a sALS MN with nuclear depletion of TDP-43 and cytoplasmic SLIs and DPSC (arrows). c) sALS MNs in ALS 40 show RLIs in the soma (arrow) and filiform aggregates in dendrites (arrowhead). d) Image of a MN showing reduced TDP-43 protein in the nucleus (arrowhead), with evident DPSC of TDP-43 (arrows). e-h) LAMP2A immunopositivity was clearly detected in the cytoplasm with a normal predominance in perinuclear localization. (i) Quantification of LAMP2A expression in ALS40 MNs showed similar levels to control MNs. (*p<0.05; **p<0,01; ***p<0.001). Abbreviations: N: Neuronal nucleus. Scale bars: a, b: 60 µm; c) 60 µm; d: 50 µm; e, f, g, h: 50 µm.

Supplementary Table 1

Supplementary Table 2

Acknowledgements
We would first like to thank the patients who participated in the clinical trials and donated their tissues, making it possible to accurately complete the pathological study of the effects of the therapy applied in each trial arm. We want to particularly acknowledge the patients and the Biobank IMIB (PT20/00109) integrated in the Platform ISCIII Biobanks and Biomodels for their collaboration and the Anatomical Innovation Unit of the UMH.

Author contributions
D.G., M.M-M., A.P., R.G-L., and D.P. contributed to the conception of the anatomopathological studies in control and ALS spinal cords. D.R. contributed to the technical work and organization of the sample collection. M.B., P.I., J.M., E.G., and S.M. participated in the clinical trials, collecting the clinical and tissue samples. G.H. collected one sALS sample and sent it to the clinical trial coordination center. R.V., together with S.M., contributed to the conception and design of the autophagy analysis. S.M. and D.G. made substantial contributions to the conception or design of the work, and to the acquisition, analysis and interpretation of data. They also drafted the work or revised it critically. All authors have approved the version to be published and agree to be accountable for all aspects of the work, ensuring that any questions related to the accuracy or integrity of any part of the work are appropriately investigated and resolved.

Funding
This work was funded by the following projects: Spanish State Research Agency, through the "Severo Ochoa" Programme for Centres of Excellence in R&D (Grant Numbers SEV-2017-0723), the Spanish Ministerio de Ciencia e Innovación grant numbers SAF2017-83702-R and PID2020-11817RB-I00 and the Generalitat Valenciana (program Prometeo II, Grant Number 2018/041). This work has been partially funded by the Instituto de Salud Carlos III (ISCIII) through the RICORS Project 'RD21/0017/0017; RD21/0017/0001; TERAV' supported by the Next Generation EU Program (Recovery, Transformation and Resilience Plan).
RV was supported by fellowship Ramon y Cajal (RYC) 2019-027520-I funded by Ministerio de Ciencia, Innovación y Universidades (MCIU) and Agencia Estatal de Investigación (AEI) MCIU/AEI/https://doi.org/10.13039/501100011033, as "European Social Fund (ESF) Investing in your future".

Data availability
No datasets were generated or analysed during the current study.

Declarations

Competing interests
The authors declare no competing interests.

Generative AI and AI-assisted technologies in the writing process
During the preparation of this work the authors used Chat-GPT to streamline some parts of the text. After using this tool, the authors reviewed and edited the content as needed and took full responsibility for the content of the publication.

Received: 24 August 2025 / Accepted: 19 January 2026
Published online: 04 February 2026

References

1. Abdrakhmanov A, Gogvadze V, Zhivotovsky B (2020) To eat or to die: Deciphering selective forms of autophagy. Trends Biochem Sci 45:347–364. https://doi.org/10.1016/j.tibs.2019.11.006
2. Andrews JA, Jackson CE, Heiman-Patterson TD, Bettica P, Brooks BR, Pioro EP (2020) Real-world evidence of riluzole effectiveness in treating amyotrophic lateral sclerosis. Amyotroph Lateral Scler Front Degener 21:509–518. https://doi.org/10.1080/21678421.2020.1771734
3. Arosio A, Cristofani R, Pansarasa O, Crippa V, Riva C, Sirtori R, Rodriguez-Menendez V, Riva N, Gerardi F, Lunetta C, Cereda C, Poletti A, Ferrarese C, Tremolizzo L, Sala G (2020) HSC70 expression is reduced in lymphomonocytes of sporadic ALS patients and contributes to TDP-43 accumulation. Amyotroph Lateral Scler Front Degener 21:51–62. https://doi.org/10.1080/21678421.2019.1672749

4. Aschenbrenner DS (2023) New drug approved for ALS. Am J Nurs 123:22–23. https://doi.org/10.1097/01.NAJ.0000911516.31267.67
5. Ayala YM, Zago P, D'Ambrogio A, Xu Y-F, Petrucelli L, Buratti E, Baralle FE (2008) Structural determinants of the cellular localization and shuttling of TDP-43. J Cell Sci 121:3778–3785. https://doi.org/10.1242/jcs.038950
6. Balaban D, Miyawaki EK, Bhattacharyya S, Torre M (2021) The phenomenon of clasmatodendrosis. Heliyon 7:e07605. https://doi.org/10.1016/j.heliyon.2021.e07605
7. Barmada SJ, Serio A, Arjun A, Bilican B, Daub A, Ando DM, Tsvetkov A, Pleiss M, Li X, Peisach D, Shaw C, Chandran S, Finkbeiner S (2014) Autophagy induction enhances TDP43 turnover and survival in neuronal ALS models. Nat Chem Biol 10:677–685. https://doi.org/10.1038/nchembio.1563
8. Barral DC, Staiano L, Guimas Almeida C, Cutler DF, Eden ER, Futter CE, Galione A, Marques ARA, Medina DL, Napolitano G, Settembre C, Vieira OV, Aerts JMFG, Atakpa-Adaji P, Bruno G, Capuozzo A, De Leonibus E, Di Malta C, Escrevente C, Esposito A, Grumati P, Hall MJ, Teodoro RO, Lopes SS, Luzio JP, Monfregola J, Montefusco S, Platt FM, Polishchuck R, De Risi M, Sambri I, Soldati C, Seabra MC (2022) Current methods to analyze lysosome morphology, positioning, motility and function. Traffic Cph Den 23:238–269. https://doi.org/10.1111/tra.12839
9. Benito-Cuesta I, Diez H, Ordoñez L, Wandosell F (2017) Assessment of autophagy in neurons and brain tissue. Cells 6:25. https://doi.org/10.3390/cells6030025
10. Blanquer M, Pérez-Espejo MA, Martínez-Lage JF, Iniesta F, Martinez S, Moraleda JM (2010) A surgical technique of spinal cord cell transplantation in amyotrophic lateral sclerosis. J Neurosci Methods 191:255–257. https://doi.org/10.1016/j.jneumeth.2010.06.014
11. Blanquer M, Moraleda JM, Iniesta F, Gómez-Espuch J, Meca-Lallana J, Villaverde R, Pérez-Espejo MÁ, Ruíz-López FJ, García Santos JM, Bleda P, Izura V, Sáez M, De Mingo P, Vivancos L, Carles R, Jiménez J, Hernández J, Guardiola J, Del Rio ST, Antúnez C, De la Rosa P, Majado MJ, Sánchez-Salinas A, López J, Martínez-Lage JF, Martínez S (2012) Neurotrophic bone marrow cellular nests prevent spinal motoneuron degeneration in amyotrophic lateral sclerosis patients: a pilot safety study. Stem Cells Dayt Ohio 30:1277–1285. https://doi.org/10.1002/stem.1080
12. Bono S, Feligioni M, Corbo M (2021) Impaired antioxidant KEAP1-NRF2 system in amyotrophic lateral sclerosis: NRF2 activation as a potential therapeutic strategy. Mol Neurodegener 16:71. https://doi.org/10.1186/s13024-021-00479-8
13. Bourdenx M, Martín-Segura A, Scrivo A, Rodriguez-Navarro JA, Kaushik S, Tasset I, Diaz A, Storm NJ, Xin Q, Juste YR, Stevenson E, Luengo E, Clement CC, Choi SJ, Krogan NJ, Mosharov EV, Santambrogio L, Grueninger F, Collin L, Swaney DL, Sulzer D, Gavathiotis E, Cuervo AM (2021) Chaperone-mediated autophagy prevents collapse of the neuronal metastable proteome. Cell 184:2696–2714e25. https://doi.org/10.1016/j.cell.2021.03.048
14. Brockington A, Ning K, Heath PR, Wood E, Kirby J, Fusi N, Lawrence N, Wharton SB, Ince PG, Shaw PJ (2013) Unravelling the enigma of selective vulnerability in neurodegeneration: motor neurons resistant to degeneration in ALS show distinct gene expression characteristics and decreased susceptibility to excitotoxicity. Acta Neuropathol (Berl) 125:95–109. https://doi.org/10.1007/s00401-012-1058-5
15. Brown RH, Al-Chalabi A (2017) Amyotrophic lateral sclerosis. N Engl J Med 377:162–172. https://doi.org/10.1056/NEJMra1603471
16. Caballero B, Wang Y, Diaz A, Tasset I, Juste YR, Stiller B, Mandelkow E-M, Mandelkow E, Cuervo AM (2018) Interplay of pathogenic forms of human Tau with different autophagic pathways. Aging Cell 17:e12692. https://doi.org/10.1111/acel.12692
17. Cajal SR (1913) y Contribución al conocimiento de la neuroglia del cerebro humano
18. Colombrita C, Onesto E, Megiorni F, Pizzuti A, Baralle FE, Buratti E, Silani V, Ratti A (2012) TDP-43 and FUS RNA-binding proteins bind distinct sets of cytoplasmic messenger RNAs and differently regulate their post-transcriptional fate in motoneuron-like cells. J Biol Chem 287:15635–15647. https://doi.org/10.1074/jbc.M111.333450
19. Cozzi M, Ferrari V (2022) Autophagy dysfunction in ALS: from transport to protein degradation. J Mol Neurosci 72:1456–1481. https://doi.org/10.1007/s12031-022-02029-3
20. Cuervo AM, Dice JF (1996) A receptor for the selective uptake and degradation of proteins by lysosomes. Science 273:501–503. https://doi.org/10.1126/science.273.5274.501
21. Cuervo AM, Stefanis L, Fredenburg R, Lansbury PT, Sulzer D (2004) Impaired degradation of mutant alpha-synuclein by chaperone-mediated autophagy. Science 305:1292–1295. https://doi.org/10.1126/science.1101738
22. Davidson YS, Raby S, Foulds PG, Robinson A, Thompson JC, Sikkink S, Yusuf I, Amin H, DuPlessis D, Troakes C, Al-Sarraj S, Sloan C, Esiri MM, Prasher VP, Allsop D, Neary D, Pickering-Brown SM, Snowden JS, Mann DMA (2011) TDP-43 pathological changes in early onset Familial and sporadic alzheimer's disease, late onset alzheimer's disease and down's syndrome: association with age, hippocampal sclerosis and clinical phenotype. Acta Neuropathol (Berl) 122:703–713. https://doi.org/10.1007/s00401-011-0879-y
23. de Boer EMJ, Orie VK, Williams T, Baker MR, De Oliveira HM, Polvikoski T, Silsby M, Menon P, van den Bos M, Halliday GM, van den Berg LH, Van Den Bosch L, van Damme P, Kiernan MC, van Es MA, Vucic S (2020) TDP-43 proteinopathies: a new wave of neurodegenerative diseases. J Neurol Neurosurg Psychiatry 92:86–95. https://doi.org/10.1136/jnnp-2020-322983
24. Deneubourg C, Ramm M, Smith LJ, Baron O, Singh K, Byrne SC, Duchen MR, Gautel M, Eskelinen E-L, Fanto M, Jungbluth H (2022) The spectrum of neurodevelopmental, neuromuscular and neurodegenerative disorders due to defective autophagy. Autophagy 18:496–517. https://doi.org/10.1080/15548627.2021.1943177
25. Deng H-X, Zhai H, Bigio EH, Yan J, Fecto F, Ajroud K, Mishra M, Ajroud-Driss S, Heller S, Sufit R, Siddique N, Mugnaini E, Siddique T (2010) FUS-immunoreactive inclusions are a common feature in sporadic and non-SOD1 Familial amyotrophic lateral sclerosis. Ann Neurol 67:739–748. https://doi.org/10.1002/ana.22051
26. Dice JF (1990) Peptide sequences that target cytosolic proteins for lysosomal proteolysis. Trends Biochem Sci 15:305–309. https://doi.org/10.1016/0968-0004(90)90019-8
27. Dice JF (2007) Chaperone-mediated autophagy. Autophagy 3. https://doi.org/10.4161/auto.4144
28. Endo Y, Furuta A, Nishino I (2015) Danon disease: a phenotypic expression of LAMP-2 deficiency. Acta Neuropathol (Berl) 129:391–398. https://doi.org/10.1007/s00401-015-1385-4
29. Fleming A, Bourdenx M, Fujimaki M, Karabiyik C, Krause GJ, Lopez A, Martín-Segura A, Puri C, Scrivo A, Skidmore J, Son SM, Stamatakou E, Wrobel L, Zhu Y, Cuervo AM, Rubinsztein DC (2022) The different autophagy degradation pathways and neurodegeneration. Neuron 110:935–966. https://doi.org/10.1016/j.neuron.2022.01.017
30. Furuta A, Wakabayashi K, Haratake J, Kikuchi H, Kabuta T, Mori F, Tokonami F, Katsumi Y, Tanioka F, Uchiyama Y, Nishino I, Wada K (2013) Lysosomal storage and advanced senescence in the brain of LAMP-2-deficient Danon disease. Acta Neuropathol (Berl) 125:459–461. https://doi.org/10.1007/s00401-012-1075-4
31. Giannini M, Bayona-Feliu A, Sproviero D, Barroso SI, Cereda C, Aguilera A (2020) TDP-43 mutations link amyotrophic lateral sclerosis with R-loop homeostasis and R loop-mediated DNA damage. PLOS Genet 16:e1009260. https://doi.org/10.1371/journal.pgen.1009260
32. Gomes C, Escrevente C, Costa J (2010) Mutant superoxide dismutase 1 overexpression in NSC-34 cells: effect of Trehalose on aggregation, TDP-43 localization and levels of co-expressed glycoproteins. Neurosci Lett 475:145–149. https://doi.org/10.1016/j.neulet.2010.03.065
33. Gonzalez Porras MA, Sieck GC, Mantilla CB (2018) Impaired autophagy in motor neurons: A final common mechanism of injury and death. Physiology 33:211–224. https://doi.org/10.1152/physiol.00008.2018
34. Guise AJ, Misal SA, Carson R, Chu J-H, Boekweg H, Van Der Watt D, Welsh NC, Truong T, Liang Y, Xu S, Benedetto G, Gagnon J, Payne SH, Plowey ED, Kelly RT (2024) TDP-43-stratified single-cell proteomics of postmortem human spinal motor neurons reveals protein dynamics in amyotrophic lateral sclerosis. Cell Rep 43:113636. https://doi.org/10.1016/j.celrep.2023.113636
35. Heckman CJ, Johnson M, Mottram C, Schuster J (2008) Persistent inward currents in spinal motoneurons and their influence on human motoneuron firing patterns. Neuroscientist 14:264–275. https://doi.org/10.1177/1073858408314986
36. Hou T, Fan Y, Dan W, Liu B, Wang Z, Zeng J, Li L (2020) Chaperone-mediated autophagy in cancer: advances from bench to bedside. Histol Histopathol 35:637–644. https://doi.org/10.14670/HH-18-202
37. Huang C-C, Bose JK, Majumder P, Lee K-H, Huang J-TJ, Huang JK, Shen C-KJ (2014) Metabolism and mis-metabolism of the neuropathological signature protein TDP-43. J Cell Sci 127:3024–3038. https://doi.org/10.1242/jcs.136150
38. Jacob SM, Lee S, Kim SH, Sharkey KA, Pfeffer G, Nguyen MD (2024) Brain-body mechanisms contribute to sexual dimorphism in amyotrophic lateral sclerosis. Nat Rev Neurol 20:475–494. https://doi.org/10.1038/s41582-024-00991-7

39. Kabeya Y, Mizushima N, Ueno T, Yamamoto A, Kirisako T, Noda T, Kominami E, Ohsumi Y, Yoshimori T (2000) LC3, a mammalian homologue of yeast Apg8p, is localized in autophagosome membranes after processing. EMBO J 19:5720–5728. https://doi.org/10.1093/emboj/19.21.5720
40. Kang K, Lee S-W, Han JE, Choi JW, Song M-R (2014) The complex morphology of reactive astrocytes controlled by fibroblast growth factor signaling. Glia 62:1328–1344. https://doi.org/10.1002/glia.22684
41. Kaplan A, Spiller KJ, Towne C, Kanning KC, Choe GT, Geber A, Akay T, Aebischer P, Henderson CE (2014) Neuronal matrix metalloproteinase-9 is a determinant of selective neurodegeneration. Neuron 81:333–348. https://doi.org/10.1016/j.neuron.2013.12.009
42. Kaushik S, Cuervo AM (2018) The coming of age of chaperone-mediated autophagy. Nat Rev Mol Cell Biol 19:365–381. https://doi.org/10.1038/s41580-018-0001-6
43. Ke YD, van Hummel A, Stevens CH, Gladbach A, Ippati S, Bi M, Lee WS, Krüger S, van der Hoven J, Volkerling A, Bongers A, Halliday G, Haass NK, Kiernan M, Delerue F, Ittner LM (2015) Short-term suppression of A315T mutant human TDP-43 expression improves functional deficits in a novel inducible Transgenic mouse model of FTLD-TDP and ALS. Acta Neuropathol (Berl) 130:661–678. https://doi.org/10.1007/s00401-015-1486-0
44. Keating SS, San Gil R, Swanson MEV, Scotter EL, Walker AK (2022) TDP-43 pathology: from noxious assembly to therapeutic removal. Prog Neurobiol 211:102229. https://doi.org/10.1016/j.pneurobio.2022.102229
45. Keller BA, Volkening K, Droppelmann CA, Ang LC, Rademakers R, Strong MJ (2012) Co-aggregation of RNA binding proteins in ALS spinal motor neurons: evidence of a common pathogenic mechanism. Acta Neuropathol (Berl) 124:733–747. https://doi.org/10.1007/s00401-012-1035-z
46. Khawaja RR, Griego E, Lindenau K, Salek A, Gambardella J, Scrivo A, Monday HR, Bourdenx M, Madero-Pérez J, Khan ZN, Chavda B, Cutler R, Graff S, Sidoli S, Santulli G, Santambrogio L, Tasset I, Kaushik S, Gan L, Castillo PE, Cuervo AM (2025) Chaperone-mediated autophagy regulates neuronal activity by sex-specific remodelling of the synaptic proteome. Nat Cell Biol 27:1688–1707
47. Khawaja RR, Martín-Segura A, Santiago-Fernández O, Sereda R, Lindenau K, McCabe M, Macho-González A, Jafari M, Scrivo A, Gomez-Sintes R, Chavda B, Saez-Ibanez AR, Tasset I, Arias E, Xie X, Kim M, Kaushik S, Cuervo AM (2025) Sex-specific and cell-type-specific changes in chaperone-mediated autophagy across tissues during aging. Nat Aging 5:691–708. https://doi.org/10.1038/s43587-024-00799-6
48. Kirchner P, Bourdenx M, Madrigal-Matute J, Tiano S, Diaz A, Bartholdy BA, Will B, Cuervo AM (2019) Proteome-wide analysis of chaperone-mediated autophagy targeting motifs. PLoS Biol 17:e3000301. https://doi.org/10.1371/journal.pbio.3000301
49. Klionsky DJ, Petroni G, Amaravadi RK, Baehrecke EH, Ballabio A, Boya P, Bravo-San Pedro JM, Cadwell K, Cecconi F, Choi AMK, Choi ME, Chu CT, Codogno P, Colombo MI, Cuervo AM, Deretic V, Dikic I, Elazar Z, Eskelinen E, Fimia GM, Gewirtz DA, Green DR, Hansen M, Jäättelä M, Johansen T, Juhász G, Karantza V, Kraft C, Kroemer G, Ktistakis NT, Kumar S, Lopez-Otin C, Macleod KF, Madeo F, Martinez J, Meléndez A, Mizushima N, Münz C, Penninger JM, Perera RM, Piacentini M, Reggiori F, Rubinsztein DC, Ryan KM, Sadoshima J, Santambrogio L, Scorrano L, Simon H, Simon AK, Simonsen A, Stolz A, Tavernarakis N, Tooze SA, Yoshimori T, Yuan J, Yue Z, Zhong Q, Galluzzi L, Pietrocola F (2021) Autophagy in major human diseases. EMBO J 40:e108863. https://doi.org/10.15252/embj.2021108863
50. Kon T, Mori F, Tanji K, Miki Y, Nishijima H, Nakamura T, Kinoshita I, Suzuki C, Kurotaki H, Tomiyama M, Wakabayashi K (2022) Accumulation of nonfibrillar TDP-43 in the rough Endoplasmic reticulum is the Early-Stage pathology in amyotrophic lateral sclerosis. J Neuropathol Exp Neurol 81:271–281. https://doi.org/10.1093/jnen/nlac015
51. Konecki DS, Foetisch K, Zimmer KP, Schlotter M, Lichter-Konecki U (1995) An alternatively spliced form of the human lysosome-associated membrane protein-2 gene is expressed in a tissue-specific manner. Biochem Biophys Res Commun 215:757–767. https://doi.org/10.1006/bbrc.1995.2528
52. Lebœuf M, Vargas-Abonce SE, Pezé-Hedsieck E, Dupont E, Jimenez-Alonso L, Moya KL, Prochiantz A (2023) ENGRAILED-1 transcription factor has a paracrine neurotrophic activity on adult spinal α-motoneurons. EMBO Rep 24:e56525. https://doi.org/10.15252/embr.202256525
53. Liao Z, Wang B, Liu W, Xu Q, Hou L, Song J, Guo Q, Li N (2021) Dysfunction of chaperone-mediated autophagy in human diseases. Mol Cell Biochem 476:1439–1454. https://doi.org/10.1007/s11010-020-04006-z
54. Longinetti E, Fang F (2019) Epidemiology of amyotrophic lateral sclerosis: an update of recent literature. Curr Opin Neurol 32:771–776. https://doi.org/10.1097/WCO.0000000000000730
55. Lu S, Hu J, Arogundade OA, Goginashvili A, Vazquez-Sanchez S, Diedrich JK, Gu J, Blum J, Oung S, Ye Q, Yu H, Ravits J, Liu C, Yates JR 3rd, Cleveland DW (2022) Heat-shock chaperone HSPB1 regulates cytoplasmic TDP-43 phase separation and liquid-to-gel transition. Nat Cell Biol 24:1378–1393. https://doi.org/10.1038/s41556-022-00988-8
56. Lunetta C, Moglia C, Lizio A, Caponnetto C, Dubbioso R, Giannini F, Matà S, Mazzini L, Sabatelli M, Siciliano G, Simone IL, Sorarù G, Toriello A, Trojsi F, Vedovello M, D'Ovidio F, Filippi M, Calvo A, EDARAVALS Study Group (2020) The Italian multicenter experience with Edaravone in amyotrophic lateral sclerosis. J Neurol 267:3258–3267. https://doi.org/10.1007/s00415-020-09993-z
57. Manastireanu DM, Salazar NA, Bejarano E, Nieto-Torres JL (2024) Selective autophagy: a therapeutic target for healthy aging? Aging adv 1:2. https://doi.org/10.4103/AGINGADV.AGINGADV-D-24-00002
58. Mannen T, Iwata M, Toyokura Y, Nagashima K (1977) Preservation of a certain motoneurone group of the sacral cord in amyotrophic lateral sclerosis: its clinical significance. J Neurol Neurosurg Psychiatry 40:464–469. https://doi.org/10.1136/jnnp.40.5.464
59. Martin LJ (1999) Neuronal death in amyotrophic lateral sclerosis is apoptosis: possible contribution of a programmed cell death mechanism. J Neuropathol Exp Neurol 58:459–471. https://doi.org/10.1097/00005072-199905000-00005
60. Masrori P, Van Damme P (2020) Amyotrophic lateral sclerosis: a clinical review. Eur J Neurol 27:1918–1929. https://doi.org/10.1111/ene.14393
61. Miller TM, Cudkowicz ME, Genge A, Shaw PJ, Sobue G, Bucelli RC, Chiò A, Van Damme P, Ludolph AC, Glass JD, Andrews JA, Babu S, Benatar M, McDermott CJ, Cochrane T, Chary S, Chew S, Zhu H, Wu F, Nestorov I, Graham D, Sun P, McNeill M, Fanning L, Ferguson TA, Fradette S, VALOR and OLE Working Group (2022) Trial of antisense oligonucleotide Tofersen for SOD1 ALS. N Engl J Med 387:1099–1110. https://doi.org/10.1056/NEJMoa2204705
62. Mori F, Yasui H, Miki Y, Kon T, Arai A, Kurotaki H, Tomiyama M, Wakabayashi K (2024) Colocalization of TDP-43 and stress granules at the early stage of TDP-43 aggregation in amyotrophic lateral sclerosis. Brain Pathol Zurich Switz 34:e13215. https://doi.org/10.1111/bpa.13215
63. Moujalled D, Grubman A, Acevedo K, Yang S, Ke YD, Moujalled DM, Duncan C, Caragounis A, Perera ND, Turner BJ, Prudencio M, Petrucelli L, Blair I, Ittner LM, Crouch PJ, Liddell JR, White AR (2017) TDP-43 mutations causing amyotrophic lateral sclerosis are associated with altered expression of RNA-binding protein HnRNP K and affect the Nrf2 antioxidant pathway. Hum Mol Genet 26:1732–1746. https://doi.org/10.1093/hmg/ddx093
64. Niedermeyer S, Murn M, Choi PJ (2019) Respiratory failure in amyotrophic lateral sclerosis. Chest 155:401–408. https://doi.org/10.1016/j.chest.2018.06.035
65. Nijssen J, Comley LH, Hedlund E (2017) Motor neuron vulnerability and resistance in amyotrophic lateral sclerosis. Acta Neuropathol (Berl) 133:863–885. https://doi.org/10.1007/s00401-017-1708-8
66. Ormeño F, Hormazabal J, Moreno J, Riquelme F, Rios J, Criollo A, Albornoz A, Alfaro IE, Budini M (2020) Chaperone mediated autophagy degrades TDP-43 protein and is affected by TDP-43 aggregation. Front Mol Neurosci 13:19. https://doi.org/10.3389/fnmol.2020.00019
67. Ovsepian SV, O'Leary VB, Martinez S (2024) Selective vulnerability of motor neuron types and functional groups to degeneration in amyotrophic lateral sclerosis: review of the Neurobiological mechanisms and functional correlates. Brain Struct Funct 229:1–14. https://doi.org/10.1007/s00429-023-02728-6
68. Paganoni S, Macklin EA, Hendrix S, Berry JD, Elliott MA, Maiser S, Karam C, Caress JB, Owegi MA, Quick A, Wymer J, Goutman SA, Heitzman D, Heiman-Patterson T, Jackson CE, Quinn C, Rothstein JD, Kasarskis EJ, Katz J, Jenkins L, Ladha S, Miller TM, Scelsa SN, Vu TH, Fournier CN, Glass JD, Johnson KM, Swenson A, Goyal NA, Pattee GL, Andres PL, Babu S, Chase M, Dagostino D, Dickson SP, Ellison N, Hall M, Hendrix K, Kittle G, McGovern M, Ostrow J, Pothier L, Randall R, Shefner JM, Sherman AV, Tustison E, Vigneswaran P, Walker J, Yu H, Chan J, Wittes J, Cohen J, Klee J, Leslie K, Tanzi RE, Gilbert W, Yeramian PD, Schoenfeld D, Cudkowicz ME (2020) Trial of sodium Phenylbutyrate-Taurursodiol for amyotrophic lateral sclerosis. N Engl J Med 383:919–930. https://doi.org/10.1056/NEJMoa1916945
69. Pajares M, Rojo AI, Arias E, Díaz-Carretero A, Cuervo AM, Cuadrado A (2018) Transcription factor NFE2L2/NRF2 modulates chaperone-mediated autophagy through the regulation of LAMP2A. Autophagy 14:1310–1322. https://doi.org/10.1080/15548627.2018.1474992

70. Park S-K, Park S, Liebman SW (2022) TDP-43 toxicity in yeast is associated with a reduction in Autophagy, and deletions of TIP41 and PBP1 counteract these effects. Viruses 14:2264. https://doi.org/10.3390/v14102264
71. Pérez-Cabello JA, Silvera-Carrasco L, Franco JM, Capilla-González V, Armaos A, Gómez-Lima M, García-García R, Yap XW, Leal-Lasarte M, Lall D, Baloh RH, Martínez S, Miyata Y, Tartaglia GG, Sawarkar R, García-Domínguez M, Pozo D, Roodveldt C (2023) MAPK/MAK/MRK overlapping kinase (MOK) controls microglial inflammatory/type-I IFN responses via Brd4 and is involved in ALS. Proc Natl Acad Sci U S A 120:e2302143120. https://doi.org/10.1073/pnas.2302143120
72. Petrov D, Mansfield C, Moussy A, Hermine O (2017) ALS clinical trials review: 20 years of Failure. Are we any closer to registering a new treatment? Front Aging Neurosci 9:68. https://doi.org/10.3389/fnagi.2017.00068
73. Qiao L, Hu J, Qiu X, Wang C, Peng J, Zhang C, Zhang M, Lu H, Chen W (2023) LAMP2A, LAMP2B and LAMP2C: similar structures, divergent roles. Autophagy 19:2837–2852. https://doi.org/10.1080/15548627.2023.2235196
74. Ramesh N, Pandey UB (2017) Autophagy dysregulation in ALS: when protein aggregates get out of hand. Front Mol Neurosci 10:263. https://doi.org/10.3389/fnmol.2017.00263
75. Riancho J, Gonzalo I, Ruiz-Soto M, Berciano J (2019) Why do motor neurons degenerate? Actualization in the pathogenesis of amyotrophic lateral sclerosis. Neurologia 34:27–37. https://doi.org/10.1016/j.nrl.2015.12.001
76. Robinson EB, Lichtenstein P, Anckarsäter H, Happé F, Ronald A (2013) Examining and interpreting the female protective effect against autistic behavior. Proc Natl Acad Sci U S A 110:5258–5262. https://doi.org/10.1073/pnas.1211070110
77. Rothaug M, Stroobants S, Schweizer M, Peters J, Zunke F, Allerding M, D'Hooge R, Saftig P, Blanz J (2015) LAMP-2 deficiency leads to hippocampal dysfunction but normal clearance of neuronal substrates of chaperone-mediated autophagy in a mouse model for Danon disease. Acta Neuropathol Commun 3:6. https://doi.org/10.1186/s40478-014-0182-y
78. Rusmini P, Cristofani R, Galbiati M, Cicardi ME, Meroni M, Ferrari V, Vezzoli G, Tedesco B, Messi E, Piccolella M, Carra S, Crippa V, Poletti A (2017) The role of the heat shock protein B8 (HSPB8) in motoneuron diseases. Front Mol Neurosci 10. https://doi.org/10.3389/fnmol.2017.00176
79. Ryu HJ, Kim J-E, Yeo S-I, Kang T-C (2011) p65/RelA-Ser529 NF-κB subunit phosphorylation induces autophagic astroglial death (Clasmatodendrosis) following status epilepticus. Cell Mol Neurobiol 31:1071–1078. https://doi.org/10.1007/s10571-011-9706-1
80. Saini A, Chawla PA (2024) Breaking barriers with tofersen: enhancing therapeutic opportunities in amyotrophic lateral sclerosis. Eur J Neurol 31:e16140. https://doi.org/10.1111/ene.16140
81. Sasaki S (2011) Autophagy in spinal cord motor neurons in sporadic amyotrophic lateral sclerosis. J Neuropathol Exp Neurol 70:349–359. https://doi.org/10.1097/NEN.0b013e3182160690
82. Schneider JL, Cuervo AM (2014) Autophagy and human disease: emerging themes. Curr Opin Genet Dev 26:16–23. https://doi.org/10.1016/j.gde.2014.04.003
83. Schweingruber C, Hedlund E (2022) The cell autonomous and Non-Cell autonomous aspects of neuronal vulnerability and resilience in amyotrophic lateral sclerosis. Biology 11:1191. https://doi.org/10.3390/biology11081191
84. Sidibe DK, Kulkarni VV, Dong A, Herr JB, Vogel MC, Stempel MH, Maday S (2022) Brain-derived neurotrophic factor stimulates the retrograde pathway for axonal autophagy. J Biol Chem 298:102673. https://doi.org/10.1016/j.jbc.2022.102673
85. Sofroniew MV, Vinters HV (2010) Astrocytes: biology and pathology. Acta Neuropathol (Berl) 119:7–35. https://doi.org/10.1007/s00401-009-0619-8
86. Suk TR, Rousseaux MWC (2020) The role of TDP-43 mislocalization in amyotrophic lateral sclerosis. Mol Neurodegener 15:45. https://doi.org/10.1186/s13024-020-00397-1
87. Valdor R, Martinez-Vicente M (2024) The role of Chaperone-Mediated autophagy in tissue homeostasis and disease pathogenesis. Biomedicines 12:257. https://doi.org/10.3390/biomedicines12020257
88. Verkhratsky A, Butt A, Li B, Illes P, Zorec R, Semyanov A, Tang Y, Sofroniew MV (2023) Astrocytes in human central nervous system diseases: a frontier for new therapies. Signal Transduct Target Ther 8:1–37. https://doi.org/10.1038/s41392-023-01628-9
89. Wang I-F, Tsai K-J, Shen C-KJ (2013) Autophagy activation ameliorates neuronal pathogenesis of FTLD-U mice: a new light for treatment of TARDBP/TDP-43 proteinopathies. Autophagy 9:239–240. https://doi.org/10.4161/auto.22526
90. Writing Group, Edaravone (MCI-186) ALS 19 Study Group (2017) Safety and efficacy of Edaravone in well defined patients with amyotrophic lateral sclerosis: a randomised, double-blind, placebo-controlled trial. Lancet Neurol 16:505–512. https://doi.org/10.1016/S1474-4422(17)30115-1
91. Xu L, Liu T, Liu L, Yao X, Chen L, Fan D, Zhan S, Wang S (2020) Global variation in prevalence and incidence of amyotrophic lateral sclerosis: a systematic review and meta-analysis. J Neurol 267:944–953. https://doi.org/10.1007/s00415-019-09652-y
92. Yoshii SR, Mizushima N (2017) Monitoring and measuring autophagy. Int J Mol Sci 18:1865. https://doi.org/10.3390/ijms18091865
93. Zhai Y, Miao J, Peng Y, Wang Y, Dong J, Zhao X (2023) Clinical features of Danon disease and insights gained from LAMP-2 deficiency models. Trends Cardiovasc Med 33:81–89. https://doi.org/10.1016/j.tcm.2021.10.012
94. Zhou X, Feliciano P, Shu C, Wang T, Astrovskaya I, Hall JB, Obiajulu JU, Wright JR, Murali SC, Xu SX, Brueggeman L, Thomas TR, Marchenko O, Fleisch C, Barns SD, Snyder LG, Han B, Chang TS, Turner TN, Harvey WT, Nishida A, O'Roak BJ, Geschwind DH, Consortium SPARK, Michaelson JJ, Volfovsky N, Eichler EE, Shen Y, Chung WK (2022) Integrating de Novo and inherited variants in 42,607 autism cases identifies mutations in new moderate-risk genes. Nat Genet 54:1305–1319. https://doi.org/10.1038/s41588-022-01148-2

Publisher's note